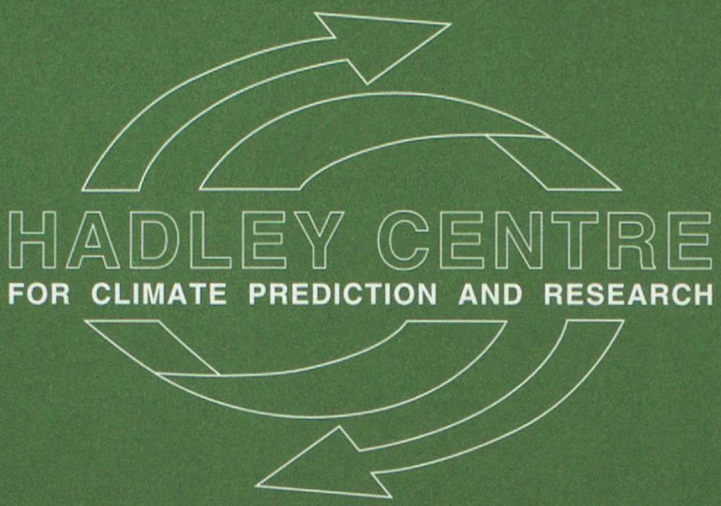

Using an Ensemble of Multi-Decadal GCM Simulations to assess Potential Seasonal Predictability

by

D P Rowell

CRTN 69

April 1996

CLIMATE
RESEARCH
TECHNICAL
NOTE

Hadley Centre
Meteorological Office
London Road
Bracknell
Berkshire RG12 2SY

CLIMATE RESEARCH TECHNICAL NOTE NO. 69

USING ANENSEMBLE OF MULTI-DEACADAL GCM SIMULATIONS TO ASSESS POTENTIAL SEASONAL PREDICTABILITY

by

D P Rowell

Manuscript submitted to *J of Climate* April 1996

Hadley Centre for Climate Prediction and Research
Meteorological Office
London Road
Bracknell
Berkshire RG12 2SY

NOTE: This paper has not been published. Permission to quote from it should be obtained from the Director of the Hadley Centre.

ABSTRACT

A global search for areas where seasonal prediction may be feasible has attracted scientific interest for many years. This paper provides a detailed contribution to this issue, based primarily on data from a 6-member ensemble of 45-year climate runs. Each run is forced by observed sea surface temperatures (SSTs) and sea-ice-extents, and is unique only in its initial atmospheric conditions. The potentially predictable component of interannual variability is assumed to be that due to oceanic forcing, and using 'analysis of variance' (ANOVA) this is separated from the unpredictable chaotic component; potential predictability is measured as the ratio of ocean-forced variance to total variance. The benefit of using ANOVA in predictability or climate variability studies is that it has been extensively used and developed for a wide range of scientific applications; the method is carefully presented here for climate modellers. A test of the null hypothesis of zero ocean impact and the calculation of confidence intervals for predictability estimates are described. The latter shows there is low susceptibility to sampling problems, owing to the large data source available. Furthermore, the limitations placed by chaotic variability on the skill of model-observed comparisons is discussed and quantified.

Global maps of potential predictability, for seasonal mean precipitation and mean sea level pressure (MSLP), are shown for 4 standard seasons. In most regions, predictability has large seasonal variations. In general, highest predictability (ie. influence of ocean forcing) occurs over the tropical oceans, particularly the Atlantic and East and Central Pacific. Land areas displaying high predictability are the Indonesian Archipelago, parts of northern South America, parts of Africa, and many tropical island regions. In the extratropics, over land, predictability is often moderate over North America, and sometimes significant, but low, over Europe and mid-latitude Asia. At polar latitudes, there is a small but significant influence of SSTs on spring MSLP. These results generally compare well with observational studies of seasonal predictability and climate variability, although a number of model errors are also uncovered.

The affects of temporal and spatial averaging on predictability are explored, and although the impact on predictability is usually positive, it can have a negative impact when the 'signal' is heterogeneous relative to the scale of averaging. Finally, the importance of interannual variations of seasonal predictability are discussed, with emphasis on the possibility of systematic variations of the seasonal mean amplitude of chaotic variability. These have a small but significant effect, although a larger ensemble is required for a full investigation.

1. Introduction

It is well known that the atmosphere behaves as a chaotic system (eg. Lorenz, 1963, 1993; Palmer, 1993a), and as a consequence deterministic predictability is limited. However, it is also well known that at many locations predictability of seasonal weather statistics is also possible (see review by Palmer and Anderson, 1994). This arises from what may be termed 'external' factors which alter the likelihood of residence in atmospheric attractors (cf. Palmer, 1993a), enabling probabilistic forecasts to be made of the seasonal mean state, on condition that the external forcing is itself predictable. The primary source of such external forcing at seasonal time-scales arises from anomalous sea surface temperature (SST) patterns; these can indeed be predicted, either using coupled dynamical models (eg. Cane et al., 1986; Barnston et al., 1994; Ji et al., 1994) or statistical models (eg. Ward et al., 1993; Barnston et al., 1994). Further potential sources of predictive skill, eg. land surface anomalies, are believed to be much less important, and are neglected through much of this paper (but see sect.7 for further discussion).

It is clearly important to be able to assess where on the globe atmospheric variations are sufficiently affected by oceanic forcing to enable practical seasonal prediction. This requires measurements of atmospheric *potential predictability* ('potential' indicates that this also depends on predictions of anomalous ocean-forcing), whose definition and mapping have been topics of ongoing research in the climate community.

To date, three basic approaches have been taken. The first involves estimating (at each point) the chaotic component of monthly or seasonal variance from a spectrum of daily data, and comparing this with the actual interannual variance of monthly or seasonal means (eg. Madden, 1976; Shukla and Gutzler, 1983; Trenberth, 1985; Zwiers, 1987; hereafter MSGT or MSGTZ). The ratio of these variances defines a measure of potential predictability which can be plotted globally. This method has the advantage that it can be based purely on observational data, since it requires only a single realisation of atmospheric evolution (although Zwiers uses a single model run). Also, it includes secondary sources of predictability, not just that due to the ocean surface. On the other hand, its assumptions (reviewed by Zwiers) include a supposition that the predictable signal is constant through each season; this will often be untrue. Furthermore, Madden also found that heterogeneous observational methods led to some erroneous predictability estimates; this may also have affected the analyses of Shukla and Gutzler (1983) and Trenberth (1985).

The second approach, adopted by Lau (1985) and Chervin (1988), compares the interannual variance of seasonal means in two runs of a general circulation model (GCM). The first run is forced by climatological SSTs in every year, and used to estimate the variance due to chaotic effects. The second run includes realistic interannual variations of SST, and provides an estimate of total interannual variance. Again, the ratio of these quantities measures potential predictability, and can be plotted as global maps. This approach requires none of the more doubtful assumptions of MSGTZ, but does rely entirely on the skill of a GCM. In particular, the models used by Lau and Chervin were less sophisticated than many available today. Furthermore, the method assumes that the interannual variance of seasonal-mean chaos is identical over a smooth climatological SST field to that over a real SST field which has systematically sharper gradients; this assumption has yet to be assessed, though may not be greatly in error.

More recently, potential predictability has been measured using an ensemble of climate simulations, where all are forced by the same observed interannually varying SSTs, but started from different initial

atmospheric conditions (Dix and Hunt, 1995; Harzallah and Sadourny, 1995; Kumar and Hoerling, 1995; Rowell et al., 1995; Stern and Miyakoda, 1995). Since these simulations provide temporally and spatially complete climate data, they are also valuable in other areas of climate research. For predictability studies, the philosophy is that sensitivity to initial atmospheric conditions can be used to quantify the chaotic component of interannual variability, whereas the relative similarity (or lack of it) between ensemble members can be used to quantify the potentially predictable component of variance. The standard statistical tool for this kind of problem is 'analysis of variance' (ANOVA), detailed in the regional study of Rowell et al. (1995), used slightly incorrectly by Harzallah and Sadourny (1995) and Kumar and Hoerling (1995) (cf. sect.2b, this paper), and used in an appropriately different form by MSGTZ. Alternative, less formal, techniques were used by Dix and Hunt (1995) and Stern and Miyakoda (1995). A particular advantage of the ensemble approach is that it is more powerful at detecting weak influences of SST (see sect.2c), but like the approach of Lau (1985) and Chervin (1988), has the potential disadvantage of relying on a model's climate skill. Arguably, this is preferable to the assumptions made in the observational approach of MSGT.

In this paper, the ensemble approach and ANOVA are used together to provide a global assessment of potential seasonal predictability. Three principal advances are made over previous ensemble studies: the use of much longer (45-year) simulations to reduce sampling error; a rigorous statistical foundation; and a detailed region-by-region analysis of predictability in each season of the year.

In sect.2, the statistical methodology and assumptions are presented for climate applications. Included is hypothesis testing, estimation of confidence intervals, and a technique for assessing the impact of chaos on model interannual skill. Sect.3 describes the model, the experiments, and the model's first- and second-moment climate statistics. In sect.4, the maps of potential seasonal predictability are described, both globally and regionally, and compared with regional observational studies. The value of these plots for climate variability studies is also emphasized. Sect.5 discusses the effects of temporal and spatial averaging on predictability, and sect.6 considers the possibility of year-to-year variations of predictability. Finally, in sect.7 conclusions and suggestions for further work are presented.

2. Statistics and Concepts

As already noted, the prime statistical tool employed in this paper is 'analysis of variance', or ANOVA. It will be used with data from an ensemble of climate simulations to separate the total atmospheric variance (σ^2_{TOT}) of some time-averaged quantity into two components, one due to oceanic (SST and sea-ice) forcing (σ^2_{SST}), and the other due to internal chaotic variability (σ^2_{INT}). Potential predictability is then measured as the ratio of ocean-forced variance to total variance ($\sigma^2_{SST} / \sigma^2_{TOT}$), having an intuitive scale of 0-100%. The main advantage of ANOVA, is that having been extensively used in other scientific applications, it is well understood and also amenable to extensions beyond its basic application. This section provides a careful presentation of ANOVA, focusing on its application to climate studies. A good statistical reference, with more in depth discussion, is Scheffe (1959).

a) Conceptual Model

First we introduce the conceptual 'model' on which the following sub-sections are based. Imagine

that data are available from an ensemble of 'n' climate simulations, each of 'N' years in length, each forced by the same varying SSTs and sea-ice, and each one differing from the others only by its initial atmospheric conditions. Consider a characteristic, 'X', which can be quantified for each individual season, eg. the time-mean of some variable at a point, a higher moment statistic, a regional index, or an EOF time coefficient. For each simulated season, this seasonal characteristic can be 'modelled' as the sum of two independent components:

$$x_{ij} = \mu_i + \varepsilon_{ij} \qquad (1)$$

where: x_{ij} = the simulated value of X

$i = 1, \ldots N$ is associated with the particular year

$j = 1, \ldots n$ is associated with the particular ensemble member

μ_i = the component of x_{ij} due to oceanic forcing (the variance of μ_i is σ^2_{SST})

ε_{ij} = the anomalous component of x_{ij} due to internal variability (the variance of ε_{ij} is σ^2_{INT})

(note, the role of land-surface forcing is dependent on the GCM and the experimental design; see sect.3)

Two key assumptions are made in the formulation and application of this 'model' (Scheffe, 1959, p222-223). The first is that the ε_{ij}'s are all randomly and independently selected from the same population. The aspect of randomness is satisfied by the inherent nature of a chaotic system so long as regime-residence times are much less than a year. Periods of atmospheric intransitivity (persistent unforced anomalies) lasting a year or more seem unlikely, not least because of the large changes of forcing associated with the passage of the annual cycle (Lorenz, 1990). The phrase, "independently selected from the same population", is used because the variance within each year of the ε_{ij}'s (σ^2_i) must be identical in all years. This is assessed in sect.6, since it is also relevant to understanding year-to-year variations of potential predictability. It suffices to note here that heterogeneity of σ^2_i is not unduly large in the data used in this paper, and furthermore that Scheffe (1959, chapter 10) notes that for a constant ensemble size such heterogeneities have little impact on the ANOVA.

The second assumption made at this stage is that the μ_i's are independently and identically distributed random variables from some defined population. This statement is valid, except where μ_i has substantial serial correlation. In these cases potential predictability is slightly underestimated (by about one quarter of its 90% confidence range), for which a bias-correction method will appear in a later paper whose specific focus is decadal variability. A further qualification for this second assumption is that it is important to identify the 'population'. In this paper it is defined as 'late twentieth century climate'. It is interesting to note that this may however be different from 'twenty-first century climate' because of anthropogenic influences; this is a pertinent issue in seasonal forecasting, since the current statistics of oceanic forcing and atmospheric response may or may not remain intact.

b) Analysis of Variance Methodology

In this sub-section we use material adapted from Rowell et al. (1995), to describe how the components of variance introduced above (σ^2_{SST} and σ^2_{INT}) can be derived from the simulation data. The brand of ANOVA used here is often described as a "one-way random-effects model".

The first step towards computing the components of variance, is to estimate the magnitude of internal variability by computing the variance of deviations from the ensemble means:

$$\hat{\sigma}^2_{INT} = \frac{1}{N(n-1)} \sum_{i=1}^{N} \sum_{j=1}^{n} (x_{ij} - \bar{x}_i)^2 \qquad (2)$$

where $\hat{y}$ denotes a best estimate of y, and:

$$\bar{x}_i = \frac{1}{n} \sum_{j=1}^{n} x_{ij} \qquad \text{(the ensemble mean of the } i^{th} \text{ year)} \qquad (3)$$

In order to estimate the variance due to oceanic forcing, it is necessary to first estimate the variance of the ensemble means:

$$\hat{\sigma}^2_{EM} = \frac{1}{N-1} \sum_{i=1}^{N} (\bar{x}_i - \bar{\bar{x}})^2 \qquad (4)$$

where:

$$\bar{\bar{x}} = \frac{1}{nN} \sum_{i=1}^{N} \sum_{j=1}^{n} x_{ij} \qquad \text{(the mean of all data)} \qquad (5)$$

Now, using a standard ANOVA result, σ^2_{EM} can be expressed in terms of σ^2_{INT} and σ^2_{SST} (eg. Scheffe, p226):

$$\sigma^2_{EM} = \sigma^2_{SST} + \frac{1}{n} \sigma^2_{INT} \qquad (6)$$

using the assumptions in sect.2a. (This result is obtained by substituting equation 1 into equation 4.) Equation 6 essentially states that the variance of the ensemble means is a *biased* estimate of the variance due to oceanic forcing. This is because with finite 'n' each ensemble mean ($\bar{x}_i$) still contains an element of internal variability (each ensemble mean is only an *estimate* of μ_i, not equal to μ_i), so that $\hat{\sigma}^2_{EM}$ overestimates σ^2_{SST}.

Thus from equations 6, 2 and 4, the variance due to oceanic forcing may be estimated as:

$$\begin{aligned} \hat{\sigma}^2_{SST} &= \hat{\sigma}^2_{EM} - \frac{1}{n} \hat{\sigma}^2_{INT} \\ &= \frac{1}{N-1} \sum_{i=1}^{N} (\bar{x}_i - \bar{\bar{x}})^2 - \frac{1}{Nn(n-1)} \sum_{i=1}^{N} \sum_{j=1}^{n} (x_{ij} - \bar{x}_i)^2 \end{aligned} \qquad (7)$$

This then leads to an estimate of the total variance:

$$\hat{\sigma}^2_{TOT} = \hat{\sigma}^2_{INT} + \hat{\sigma}^2_{SST} \qquad (8)$$

and finally, to the ratios of these variance estimates:

$$\frac{\hat{\sigma}^2_{SST}}{\hat{\sigma}^2_{TOT}} \quad \text{and} \quad \frac{\hat{\sigma}^2_{INT}}{\hat{\sigma}^2_{TOT}} \qquad (9)$$

The former of these variance ratios will be used in sects.4-6 to measure potential predictability, and so it is convenient to define:

$$\rho = \frac{\sigma^2_{SST}}{\sigma^2_{TOT}} \qquad (10)$$

Note that ρ should always be viewed as some kind of 'average' impact of oceanic forcing over *all* years. In sect.6, the possibility that the relative influence of boundary forcing in any single year may be significantly larger or smaller than this 'average' will be addressed. Furthermore, it should also be noted that $\hat{\sigma}^2_{SST}/\hat{\sigma}^2_{TOT}$ is a slightly biased estimate of ρ, since in general $E(a/b) \neq E(a)/E(b)$, where E(y) is the expectation of y. Donoghue and Collins (1990) show how to correct this bias of ρ, and for the data to be

analysed here (N=45, n=6), it is found to be negatively biased by up to 0.014. Since this is considerably less than the sampling error (sect.2d), and to simplify the mathematics of the following sub-sections, we equate $\hat{\sigma}^2_{SST}/\hat{\sigma}^2_{TOT}$ and $\hat{\rho}$, and note that this has only a minor impact on the plotted estimates of ρ in sects.4 and 5. For smaller datasets this bias is a little larger; eg. for N=11, n=9 (cf. Kumar and Hoerling, 1995), ρ is negatively biased by up to 0.059, but this is still only about one seventh of the 90% confidence range.

It is also worth mentioning at this stage two pitfalls which may occur in the application of the above equations. First, because equation 7 involves a subtracted term, the *distribution* of $\hat{\sigma}^2_{SST}$ includes a few negative values, which may sometimes be produced by chance. This is likely however only when n and N are small *and* when ρ is small. These negative values should be reset to zero (before being used in equations 8 and 9). Second, it may be a tempting shortcut to estimate σ^2_{TOT} as: $\frac{1}{Nn-1}\sum_{i=1}^{N}\sum_{j=1}^{n}(x_{ij} - \bar{\bar{x}})^2$. However, this is a *biased* estimate of σ^2_{TOT}, because it fails to account for the impact that ρ has on the 'amount of information' available (eg. if $\rho=0$, then Nn independent values of x_{ij} are available to estimate σ^2_{TOT}, whereas if ρ is large, the x_{ij}'s are interdependent, affecting the degrees of freedom and hence the calculation of σ^2_{TOT}). So in general, the total variance is correctly estimated only by the *sum of its two components* (ie. equation 8). Indeed, all computations of total variance from ensemble data should follow this method, whether or not there is an intention to study the variance components.

c) Testing a Null Hypothesis

We now consider the test of a basic hypothesis which in sect.4 will enable us to determine which parts of the globe we can be certain (within a given level of significance) that oceanic forcing has had at least some impact on interannual climate variability. The null hypothesis for a particular point or region is:

$$H_0 : \sigma^2_{SST} = 0 \quad , \quad \text{or} \quad \rho = 0 \qquad (11)$$

(which is equivalent to a hypothesis that population means for all years are identical, ie. $\mu_i = \mu$, for all i).

An additional assumption required in this sub-section (beyond those already noted) is that the anomalies due to internal variability (ε_{ij}) derive from a Gaussian distribution. It is emphasized that prior to this point (and in sect.2e), no assumptions were made about the distributions from which the data were derived. In order to check the validity of this Gaussian assumption, 270 simulated values of the quantity $x_{ij} - \bar{x}_i$ (i=1, ..., 45; j=1, ..., 6; see sect.3b for experimental design) were computed for seasonal mean sea-level pressure (MSLP) and seasonal precipitation at each grid point, and then tested against the null hypothesis of a Gaussian distribution using a Kolmogorov-Smirnov (KS) test (eg. Hoel, 1971; Press et al., 1992) and a χ^2 test. For seasonal MSLP, the null hypothesis is rejected at the 5% level over only 0.2% and 5% of the globe (KS and χ^2 tests, respectively; percentage is an average of 4 seasons), and since occasional rejection is expected by chance, we can reasonably suppose the entire data to be near-Gaussian. For seasonal precipitation, however, the null hypothesis is rejected over 14% and 23% of the globe (KS and χ^2 tests, respectively), with areas of rejection being mainly over arid regions. This pattern of rejection is expected, since a typical season in these areas contains only a few precipitation events, resulting in a highly skewed distribution of anomalies. However, if instead the logarithm of precipitation is used, the null

hypothesis is then only rejected over 1% and 8% of the globe (KS and χ^2 tests, respectively), and again we can suppose that much or all of the data is near-Gaussian. Thus in sect.4, the hypothesis of $\sigma^2_{SST} = 0$ is tested using log-precipitation data, rather than 'raw' precipitation.

Returning to equation 11, we shall now determine a criterion at which this null hypothesis can be rejected for a given level of significance. If the hypothesis is true, then the total variance can be estimated in two ways. First:

$$\sigma^2_{TOT} = \sigma^2_{INT} \qquad \text{(from equation 8, knowing } \sigma^2_{SST} = 0) \tag{12}$$

and, second, using the equation for the variance of 'n' data sampled at random from a population:

$$\sigma^2_{EM} = \frac{\sigma^2_{TOT}}{n} \tag{13}$$

$$\therefore \sigma^2_{TOT} = n\sigma^2_{EM}$$

(note that it is acceptable under the null hypothesis that each sample is actually made up of data from the same year, rather than having been sampled completely at random from the entire population).
Combining equations 12 and 13 gives:

$$n\sigma^2_{EM} = \sigma^2_{INT} \quad , \qquad \text{under } \mathbf{H_0} \tag{14}$$

Estimates of each of these variances can be obtained from the experimental data, and then the possibility that they derive from the same population (ie. the null hypothesis is true), can be assessed using Fisher's F-test. Under $\mathbf{H_0}$, the ratio of the two estimates follows a central F distribution. Thus:

$$\Pr\left\{ \frac{n\hat{\sigma}^2_{EM}}{\hat{\sigma}^2_{INT}} > F_{[N-1,\,N(n-1)],\,\alpha} \right\} = \alpha \quad , \qquad \text{under } \mathbf{H_0} \tag{15}$$

where $F_{[\nu_1,\nu_2],\,\alpha}$ is the F-statistic at the α significance level, with degrees of freedom ν_1 and ν_2. (Note that under the null hypothesis, serial correlation is estimated as zero, and so has no effect on the number of degrees of freedom.) It is the application of this test that requires the ε_{ij}'s derive from a Gaussian distribution.

The criterion for rejecting $\mathbf{H_0}$ at the α significance level is then:

$$\frac{n\hat{\sigma}^2_{EM}}{\hat{\sigma}^2_{INT}} > F_{[N-1,\,N(n-1)],\,\alpha} \tag{16}$$

Note that this is a one-sided test, since it is known that if $\mathbf{H_0}$ is rejected, $n\sigma^2_{EM} > \sigma^2_{INT}$.

In sect.4, this rejection criterion will be required in terms of $\hat{\rho}$. To reformulate equation 16, we define:

$$\hat{\beta} = \frac{n\hat{\sigma}^2_{EM}}{\hat{\sigma}^2_{INT}} \tag{17}$$

and also use:

$$\hat{\beta} = 1 + n(\hat{\rho}^{-1} - 1)^{-1} \tag{18}$$

$$\hat{\rho} = (1 + n(\hat{\beta} - 1)^{-1})^{-1} \tag{19}$$

which are easily derived from equations 6, 8, 10 and 17.
Thus from equations 16, 17 and 19, the criterion for rejecting $\mathbf{H_0}$ at the α significance level is alternatively:

$$\hat{\rho} > (1 + n(F_{[N-1,\,N(n-1)],\,\alpha} - 1)^{-1})^{-1} \tag{20}$$

d) Estimation of Confidence Intervals

In this sub-section confidence intervals for ρ are derived and plotted; these will be referred to in sect.4, where maps of $\hat{\rho}$ are displayed.

A further assumption, required only for this sub-section, is that the ensemble means ($\overline{x}_i$'s) have also been sampled from a Gaussian distribution. For large ensembles, this is automatically valid under the central limit theorem, but for small ensembles, such as used here (n=6), its validity should be tested. 45 simulated values of $\overline{x}_i$ (i=1, ..., 45; see sect.3b for experimental design) were computed for seasonal MSLP and seasonal precipitation at each grid point, and tested against the null hypothesis of a Gaussian distribution using a KS test and a χ^2 test. Not surprisingly, the MSLP data can again be accepted as Gaussian, with only 0.1% and 5% of the globe rejected at the 5% level (KS and χ^2 tests, respectively; percentages are an average of 4 seasons). For precipitation, the primary limitation to estimating confidence intervals is that the deviations of precipitation from their ensemble means are non-Gaussian over arid regions (sect.2c). There are two ways of resolving this: the first is to simply view with caution the confidence intervals over arid regions, and the second is to perform all analyses, including variance separation, on the logarithm of precipitation. The former approach is adopted in sect.4, since 'actual' precipitation is more readily understood than its logarithm.

Now, to derive confidence intervals for ρ, we define these as ρ_a and ρ_b, such that:

$$\rho_a < \rho < \rho_b , \quad \text{with probability } 1-\alpha \tag{21}$$

which can also be written:

$$\Pr\{\rho < \rho_a\} = \alpha/2 \tag{22}$$

$$\Pr\{\rho > \rho_b\} = \alpha/2 \tag{23}$$

To compute ρ_a, it is helpful to consider the distribution of a variable $\hat{\rho}_a$, for which each point on the distribution is a predictability estimate from sampled data whose true predictability is ρ_a. An inequality which occurs with the same probability as that expressed in equation 22, is:

$$\Pr\{\hat{\rho}_a > \hat{\rho}\} = \alpha/2 \tag{24}$$

We now consider further the distribution for which $\rho = \rho_a$, with the aim of deriving an inequality of the form $\Pr\{\hat{\rho}_a > f(\rho_a)\} = \alpha/2$. Then by comparison with equation 24, it will be possible relate ρ_a to $\hat{\rho}$. As a first step, note that $\rho = \rho_a$ is equivalent to:

$$\sigma^2_{SST} = \rho_a \sigma^2_{TOT} \tag{25}$$

Next, this is reformulated in terms of σ^2_{EM} and σ^2_{INT}, since we know the ratio of estimates of these variances follows an F distribution with known degrees of freedom. This involves defining a parameter β_a, related to ρ_a in an analogous way to equations 18 and 19, and so writing:

$$n\,\sigma^2_{EM} = \beta_a \sigma^2_{INT} \tag{26}$$

To obtain the inequality which can be related to equation 24, we find the point on this F distribution which is exceeded with probability $\alpha/2$:

$$\Pr\left\{ \frac{n\,\hat{\sigma}_{a\,EM}^{2}}{\beta_a\,\hat{\sigma}_{a\,INT}^{2}} > F_{[N-1,\,N(n-1)],\,\alpha/2} \right\} = \alpha/2 \qquad (27)$$

After relating $n\,\hat{\sigma}_{a\,EM}^{2}/\beta_a\,\hat{\sigma}_{a\,INT}^{2}$ to $\hat{\rho}_a$ and ρ_a (using equations 17 to 19), some straightforward manipulation gives:

$$\Pr\{\ \hat{\rho}_a > (n(F_{[N-1,\,N(n-1)],\,\alpha/2}(1+n(\rho^{-1}{}_a-1)^{-1})-1)^{-1}+1)^{-1}\ \} = \alpha/2 \qquad (28)$$

Thus comparing equations 24 and 28:

$$\hat{\rho} = (n(F_{[N-1,\,N(n-1)],\,\alpha/2}(1+n(\rho^{-1}{}_a-1)^{-1})-1)^{-1}+1)^{-1} \qquad (29)$$

and inverting this:

$$\rho_a = (n(F^{-1}_{[N-1,\,N(n-1)],\,\alpha/2}(1+n(\hat{\rho}^{-1}-1)^{-1})-1)^{-1}+1)^{-1} \qquad (30)$$

Similarly, to obtain ρ_b, the step from equation 22 to equation 24 is analogous to replacing equation 23 with the expression:

$$\Pr\{\hat{\rho}_b < \hat{\rho}\} = \alpha/2\ , \quad \text{if} \quad \rho = \rho_b \qquad (31)$$

Following equations 24 to 27, and noting that the sign of the inequality is reversed, a relationship corresponding to equation 27 is:

$$\Pr\left\{ \frac{n\,\hat{\sigma}_{b\,EM}^{2}}{\beta_b\,\hat{\sigma}_{b\,INT}^{2}} < \frac{1}{F_{[N(n-1),\,N-1],\,\alpha/2}} \right\} = \alpha/2 \qquad (32)$$

Thus, continuing to duplicate the above manipulation (equations 27 to 30):

$$\rho_b = (n(F_{[N(n-1),\,N-1],\,\alpha/2}(1+n(\hat{\rho}^{-1}-1)^{-1})-1)^{-1}+1)^{-1} \qquad (33)$$

Note that when computing ρ_a and ρ_b, the value of $\hat{\rho}$ should be obtained *without* resetting negative values of $\hat{\sigma}^2_{SST}$ to zero; this is explained below.

These confidence intervals for ρ are displayed in Fig.1 for various sized ensembles, for 10-year experiments such as AMIP (Atmospheric Model Intercomparison Project; Gates, 1992), and for 45-year experiments, such as those used in sects.4-6 of this paper. (Note that in practice the number of years should strictly be replaced by an 'effective' number of years, which would allow for the effects of serial correlation on the degrees of freedom; this always widens the limits, and of course varies spatially.) The following paragraphs interpret these plots.

First, consider the negative values. Data plotted on the abscissa are values of $\hat{\rho}$ calculated *without* resetting negative $\hat{\sigma}^2_{SST}$ to zero (mentioned above); however, consistent with the arguments of sect.2b, the 'best estimate' in such cases is plotted as zero. For the estimation of confidence intervals in these circumstances, Scheffe (1959, p230) notes that "most users of confidence intervals have a more or less conscious feeling that the length of a two-sided confidence interval is a measure of the error of some point estimate of the parameter", and "... if the interval is considerably shortened by deleting the part, if any, to the left of the origin [ie. below the origin in Fig.1], a misleading impression of accuracy of the estimation may result". Hence he suggests that negative values of ρ_a or ρ_b are *not* modified, and following this argument we plot these uncorrected on Fig.1, against the uncorrected values of $\hat{\rho}$ from which they have been derived. Of course when the upper interval is less than zero, this indicates that the associated value of $\hat{\rho}$ is actually rather unlikely to occur in practice. Taken to the extreme, an absolute lower limit for $\hat{\rho}$

is evident from equation 19; since $\hat{\beta}$ is positive definite ($\hat{\sigma}^2_{EM} \geq 0$ and $\hat{\sigma}^2_{INT} \geq 0$), this limit is $\hat{\rho} \geq (1 - n)^{-1}$.

Not surprisingly, as the ensemble size increases, the accuracy of estimates of ρ are enhanced. Fig.1 also shows confidence intervals for the limiting case of an infinite ensemble. A finite separation still remains between upper and lower intervals, becoming more pronounced with fewer years, which is because the accuracy with which σ^2_{EM} can be estimated is limited by the number of years. To a large extent this limitation also determines the magnitude of the confidence intervals for finite-sized ensembles. Thus for accurate estimates of ρ, it is important to have simulations extending over many years as well as a reasonable sized ensemble.

A further application of Fig.1, besides assessing maps or single values of ρ, might be as a partial aid to experimental design. For example, for a predetermined computing resource, and a primary aim of obtaining maximally accurate estimates of the overall contribution of oceanic forcing to climate variability, one could deduce from Fig.1 the ideal balance between ensemble size (n) and ensemble length (N). Note though, that the solution varies with ρ. For other objectives however, this may not be the best approach to experimental design; for example, if the main focus is the impact of SSTs on the probability distribution of long-lived weather regimes, resources might be better invested into larger ensembles for fewer years.

As a final comment for this sub-section, it can also be shown that equation 29 provides a rejection criterion for an alternative null hypothesis: $\rho < \rho_a$. This criterion is that if $\hat{\rho}$ is greater than the right-hand-side of equation 29, then the null hypothesis is rejected at the $\alpha/2$ significance level (if $\rho_a = 0$, this is also equivalent to the rejection criterion of H_ϕ, equation 11). An assessment of $\rho < \rho_a$ could be useful if, for example, a seasonal prediction scheme requires that a particular level of potential SST-induced skill is achievable before the scheme can be considered viable.

e) Relationship with Correlation Skill

Supposing one computes the correlation between the time series from two individual runs, it is expected that this would be related to the portion of random variability present in each series; for example, the lower the value of ρ, the lower the correlation between the runs (we shall denote the population value of this correlation by 'r'). Next, suppose that a perfect model is available, and a time series from a single run of this model is correlated instead with an observed time series. This correlation would also estimate r, and have the same relationship with ρ, ie. it to would be strongly affected by the magnitude of chaotic variability. For a non-perfect model, this correlation with an observed time series would in general be *limited* by this function of ρ. Thus if the skill of a model's interannual variability is to be properly evaluated, an understanding of this relationship is essential. It is the purpose of this sub-section to mathematically relate ρ and r. Only the assumptions of sect.2a are required.

First, the correlation between time series from two runs, j=1 and j=2, can be written as:

$$\hat{r} = \frac{\sum_{i=1}^{N} (x_{i1} - [x]_1)(x_{i2} - [x]_2)}{\left(\sum_{i=1}^{N} (x_{i1} - [x]_1)^2 \sum_{i=1}^{N} (x_{i2} - [x]_2)^2 \right)^{\frac{1}{2}}} \qquad (34)$$

where:

$$[x]_j = \frac{1}{N}\sum_{i=1}^{N} x_{ij} \tag{35}$$

This is also analogous to the correlation between an observed time series and a perfect-model time series. (Note that the explicit identification of individual runs here is not intended to indicate a unique character to each run, and the assumption of entirely random ε_{ij}'s still stands.) Substituting equation 1 into the numerator of equation 34, and multiplying the denominator by a factor (N-1)/(N-1), we obtain:

$$\hat{f} = \frac{\sum_{i=1}^{N} (\mu_i + \varepsilon_{i1} - \mu - [\varepsilon]_1)(\mu_i + \varepsilon_{i2} - \mu - [\varepsilon]_2)}{(N-1)\left(\frac{1}{N-1}\sum_{i=1}^{N}(x_{i1} - [x]_1)^2\right)^{\frac{1}{2}}\left(\frac{1}{N-1}\sum_{i=1}^{N}(x_{i2} - [x]_2)^2\right)^{\frac{1}{2}}} \tag{36}$$

Next, the numerator is expanded, and the denominator simplified by noting that $\frac{1}{N-1}\sum_{i=1}^{N}(x_{ij} - [x]_j)^2$ is an unbiased estimator of σ^2_{TOT} (the possibility of a biased estimate of σ^2_{TOT}, noted in sect.2b, does not apply here, since with n=1 the 'amount of information' is not affected by the data structure):

$$\hat{f} = \frac{\sum_{i=1}^{N}(\mu_i - \mu)^2 + \sum_{i=1}^{N}(\mu_i - \mu)(\varepsilon_{i1} - [\varepsilon]_1 + \varepsilon_{i2} - [\varepsilon]_2) + \sum_{i=1}^{N}(\varepsilon_{i1} - [\varepsilon]_1)(\varepsilon_{i2} - [\varepsilon]_2)}{(N-1)\,\hat{\sigma}_{TOT}\,\hat{\sigma}_{TOT}} \tag{37}$$

The first term of the numerator is now simply $(N-1)\,\hat{\sigma}^2_{SST}$, the second term is estimated by zero since the 'signal' due to oceanic forcing is uncorrelated with chaotic 'noise' (first assumption, sect.2a), and the third term is also estimated by zero since the chaotic variations are uncorrelated between runs (also first assumption, sect.2a). Hence:

$$\hat{f} = \frac{\hat{\sigma}^2_{SST}}{\hat{\sigma}^2_{TOT}} \tag{38}$$

Thus the inter-run correlation is actually equivalent to the portion of variance due to oceanic forcing (apart from the small bias noted towards the end of sect.2b). Hence, following the discussion above, it can be seen that the correlation between an observed time series and a single model time series is limited by ρ (assuming the model estimate of ρ is correct).

A minor extension of this is that if an ensemble of n model realisations is available, and one correlates each of these with an observed time series, then the average of these n correlations is also limited by ρ (since each individual correlation is limited by ρ). This idea will be used in sect.5. In a similar vein, Dix and Hunt (1995) use an average of correlations between all possible pairs of runs as an estimate of "areas where a systematic relationship [with SSTs] can be expected"; since each correlation estimates ρ, then the average also estimates ρ, and their diagnostic then turns out to be equivalent to the ANOVA approach described here.

An approach perhaps more often taken with ensembles, is to correlate the observed time series with ensemble means rather than with individual runs. This is expected to be more skilful, since much of the model's chaotic variability is averaged out. We shall therefore now derive the limit imposed on this correlation by the chaotic variability remaining (mainly) in the observed data. Since in this limit the model is assumed to be perfect, the observed time series can simply be viewed as an additional run, which is added to an existing ensemble of n model runs. We shall label this extra run 'A', and correlate its time series with the ensemble mean time series of the model runs:

$$\hat{f}_{EM} = \frac{\sum_{i=1}^{N} (x_{iA} - [x]_A)(\bar{x}_i - \bar{\bar{x}})}{\left(\sum_{i=1}^{N} (x_{iA} - [x]_A)^2 \sum_{i=1}^{N} (\bar{x}_i - \bar{\bar{x}})^2 \right)^{\frac{1}{2}}} \quad (39)$$

After substituting equation 1 (cf. equation 34 to 36), an expansion of the numerator can be shown to give the same result as before, but the denominator now differs (cf equation 36 to 37):

$$\hat{f}_{EM} = \frac{\hat{\sigma}^2_{SST}}{\hat{\sigma}_{TOT}\,\hat{\sigma}_{EM}} \quad (40)$$

Using equations 6 and 8, and ignoring the small bias in estimates of ρ (sect.2b), this can be written:

$$\hat{f}_{EM} = \hat{\rho}\, n^{1/2} \left(\hat{\rho}\,(n - 1) + 1 \right)^{-1/2} \quad (41)$$

Thus, this represents the *maximum* value one would anticipate for a correlation between observed data and the ensemble means of model data. As expected, $\hat{f}_{EM} > \hat{f}$ for $n>1$ (unless $\hat{\rho}=1$), and $\hat{f}_{EM} = \hat{f}$ for $n=1$. Also note that as $n \to \infty$, so $\hat{f}_{EM} \to \hat{\rho}^{1/2}$. One can also envisage using this result as part of a new skill score which would compare actual correlations with this maximum correlation, and so have the property of being unaffected by spatial heterogeneities of chaos. An important caveat however, is that such a score would inherently assume that the model estimate of ρ is a realistic estimate of ρ in the real atmosphere; this may not always be true.

3. Model and Experimental Design

a) Model Formulation

The GCM used in this paper is known as HADAM1, the first version of the HADley Centre Atmospheric Model, and is identical to that submitted to AMIP in 1993 (the Atmospheric Model Intercomparison Project, Gates, 1992). It is a grid point model with a horizontal resolution of 2.5° latitude by 3.75° longitude and 19 hybrid levels in the vertical. Physical parameterizations include: a gravity wave drag scheme; a radiation scheme which computes fluxes in four long-wave bands and six short-wave bands, and responds to prognostic cloud variables (large-scale cloud amount, cloud liquid-water and ice content, and convective cloud amount); a penetrative convection scheme with stability dependent closure, which represents both updrafts and downdrafts; boundary layer mixing in up to five of the lowest model layers; a land surface scheme which includes a vegetation canopy model, a four-layer soil model for heat conduction, and a single-layer soil model for moisture storage including surface and sub-surface runoff. The GCM's chemistry involves seasonally and meridionally varying ozone profiles, and a fixed carbon dioxide concentration (321ppmv). The background behind the model development is given by Cullen (1993), and a detailed summary of the physics and dynamics of the precise version used here is provided by Phillips (1994) and references therein.

A feature of the model, of particular relevance to the interpretation of the ANOVA results presented in later sections, is that its heat and moisture contents over the land surface interact freely with the model atmosphere, and therefore the interannual variability of the land surface (and its effect on the atmosphere) is incorporated within the chaotic component of variance. In future studies, it might also be desired to consider the influence of the land surface as *an agent which contributes to the forcing* of

atmospheric variability, rather merely as *an internal component of a (partially) forced system*. In the former case, the model should be set-up with prescribed heat and moisture fluxes over the global land surface, and ANOVA techniques could then be applied following sect.2, to separate land surface forced variability and internal atmospheric variability.

b) Experimental design

The philosophy behind an ensemble approach to GCM experimental design was discussed in sect.1. The particular suite of experiments utilised in this paper consists of an ensemble of six 45-year integrations, forced throughout by observed SST and sea-ice data. In the notation of sect.2, we thus have N=45 and n=6. Each integration runs from 00Z 1 October 1948 to 00Z 1 December 1993, with the first two months of each run being discarded because of possible spin-up effects as the model atmosphere evolves from its initial state to one in quasi-equilibrium with the imposed SSTs. The initial atmospheric conditions were all chosen arbitrarily from recent UK Meteorological Office operational analyses, but for a date close to 1 October: 1-10-91, 1-10-92, 2-10-92, 3-10-92, 1-10-93, and 2-10-93. For all runs, soil moisture and snow depth were initialised from an adaptation of Willmott et al.'s (1985) climatologies, soil surface temperature was initialised from the same operational analyses as the atmosphere, and deep soil temperatures were initialised using equations taken from Warrilow et al. (1986).

The observed ocean surface data used to force the GCM is the first version (1.1) of the specifically designed GISST (Global sea-Ice and Sea Surface Temperature) data set, described by Parker et al. (1995). The raw GISST data, available as monthly means on a 1° by 1° grid, were interpolated to the model grid as follows: model grid-boxes in the open ocean and those with up to 50% ice cover, were set as sea points with a temperature determined by the area-weighted average of non-ice 1° squares; model grid-boxes with greater than 50% ice cover were specified as ice points. The data were then enhanced temporally, by linear interpolation to 5-day means, so as to obtain a smoother evolution of boundary forcing.

c) Model Climatology

An assumption inherent in this paper (and most modelling papers), is that the GCM provides an accurate representation of the real atmosphere. Before using this model to assess predictability, it is important to consider the validity of this assumption. A number of studies have recently reviewed and compared the global performance of GCMs: eg. Fiorino (1995), Frederiksen et al. (1995), Gates et al. (1995). In particular, the model used here was ranked close to the top of those submitted to AMIP in 1993/94, using a variety of objective measures of mean climate and variability (M.Fiorino, personal communication, 1995), and can thus be regarded as 'state-of-the-art'. However, no model is without deficiencies, and it is the aim of this sub-section to assess some of the strengths and weaknesses of HADAM1, so as to aid interpretation of results presented in later sections. The focus is on the mean climate and interannual standard deviation of MSLP and precipitation, the main variables of interest in this paper. Table 1 shows spatial correlation coefficients between area-weighted observed and model fields, and Fig.2 shows example maps of the model's mean climate with its difference from observations; these maps are restricted to DJF and JJA for reasons of space.

For MSLP, Table 1 shows that the model compares very well with the near-global data of Basnett

and Parker (1995). Errors which should be noted are as follows (see also Fig.2a,b): the subtropical highs are a little too intense, the Antarctic circumpolar trough too deep, the Aleutian low too deep (except JJA), the Icelandic low extends a little too far south in winter, and the Siberian winter high is too weak. Given the focus of this paper on variability, Table 1 (second row) also verifies the model's pattern of its interannual standard deviation ($\hat{\sigma}_{TOT}$, from equation 8). Although skill is a little lower than for the mean fields, it is still encouragingly high. The main errors (not shown) are as follows: too little variability in the Antarctic circumpolar trough from South America eastward to New Zealand, an apparent excess of variability at similar latitudes in the Pacific hemisphere during JJA and SON (this may however reflect a likely negative bias in the estimated observed variability of the extratropical southern hemisphere, D.E.Parker, personal communication, 1995), a lack of winter variability over the high latitudes of Eurasia, and a small positive bias over much of the remainder of the globe.

The precipitation fields are verified in Table 1 on a degraded grid of 5° latitude by 7.5° longitude, consistent with other sections of this paper (explained in sect.5), and compared with the globally-complete data of Legates and Willmott (1990) and an updated version of the terrestrial data of Hulme (1994). When degrading the resolution of the Hulme data (originally on the same grid as the model), each 5° by 7.5° box was formed as an average of all the 2.5° by 3.75° boxes within it, and set to missing only if all four of the smaller boxes were missing; data-coverage within the verification area was thus 43% (area-weighted), compared with 100% for the Legates-Willmott data. The results of Table 1 suggest that simulation of precipitation patterns is a more exacting task for the model than the simulation of MSLP. There are likely three reasons for this; first that the model resolution is inadequate to fully resolve strong topographic effects on precipitation, second that precipitation has higher spatial gradients than MSLP so small positional errors have a greater impact on pattern correlation, and third that observations of precipitation are less certain, particularly over the oceans. The latter of these points may in part explain the greater propensity of model-observed differences over oceanic areas (Fig.2c,d). These include: higher model rainfall over the tropical northwest Pacific, less rainfall further south over the equatorial west Pacific (particularly JJA), lower rainfall in the east Pacific ITCZ (except MAM), a more marked SPCZ (all seasons), higher rainfall in the Bay of Bengal and the eastern Arabian Sea in JJA, and seasonally varying differences in the location the Atlantic ITCZ. Over continental regions, the observed data should be fairly accurate. Model errors here include the following: a wet bias over the Andes, a dry bias further east over much of the remainder of northern South America, wet biases over southern Africa (except JJA), a wet bias over Australia in DJF, and too little summer rainfall over eastern Europe, western Asia and much of southern Asia. Despite these errors, it should be further emphasized that the overall pattern correlations are still reasonable at around 0.7. The interannual standard deviation of rainfall can only be evaluated against the terrestrial time-dependent data of Hulme. Its pattern simulation skill is close to that for mean rainfall (Table 1), and the model-observed difference patterns (not shown) are also similar; this arises because precipitation is zero-bounded field, yielding a close relationship between its mean and variance.

In summary, although like all GCMs this model has some significant errors, it does in general provide a reasonable representation of the real atmosphere, and so with appropriate caution can be used as a valuable tool for studying potential seasonal predictability.

4. Where is the Impact of Ocean Forcing Largest?

As a first application of the techniques presented in sect.2, maps of 'seasonal potential predictability', ρ, are presented in Figs.3 and 4. These have been computed by applying, at each grid point, the analysis of variance to the six 45-year runs, and taking seasonal-mean precipitation or seasonal-mean MSLP (mean sea-level pressure) as the 'seasonal characteristic' whose variability is being assessed (ie. X in sect.2a). (Note that the raw precipitation data were first degraded to a resolution of 5° latitude by 7.5° longitude, by averaging over clusters of four grid-boxes; see also sect.5.) Shown in white are areas of insignificant potential predictability, which satisfy the null hypothesis of sect.2c. An important point in the interpretation of these maps, also mentioned in sect.1, is that they represent *potential predictability* only under the assumption that this derives entirely from oceanic forcing; the possibility of further predictive skill from knowledge of the pre-season land surface or atmospheric state, or from the effects of other forcings, is neglected (see also sect.7). Furthermore, and although strictly speaking this potential for prediction is realised only if the ocean surface itself can be predicted, for simplicity the terms 'predictability' and 'potential predictability' are now used interchangeably. Finally, it is also re-emphasized that the maps in Figs.3 and 4 represent an 'average' measure of predictability for the 45 years; sect.6 will consider the possibility of year-to-year variations around this measure.

Not surprisingly, the overall impression of these plots exhibits a strong impact of SSTs in the tropics, where large-scale SST anomalies can substantially affect the large-scale atmospheric modes, which in turn are more linear and hence less chaotic (cf. Charney and Shukla, 1981; Palmer and Anderson, 1994). Conversely the plots also reflect the much more chaotic nature at higher latitudes, where non-linear dynamical flow instabilities are generally larger. It is striking however, that despite the largely chaotic nature of vast areas of the globe, oceanic forcing still has a significant (albeit often small) influence on interannual variability; for precipitation, ρ is significantly greater than zero for 79%, 82%, 80% and 80% of the globe for DJF, MAM, JJA and SON respectively, and for MSLP, 83%, 88%, 85% and 89% of the globe (note, this calculation accounts for the diminishing size of grid-boxes at higher latitudes). A degree of potential seasonal predictive power exists then even for many mid-latitude regions, and although this is certainly not deterministic, if realised it could still benefit those 'customers' able to profit from probabilistic forecasts. Last, it is also noteworthy that in many regions there is a substantial annual cycle of predictability, which emphasizes the need to seasonally stratify any analysis of this nature.

Regional patterns of predictability are now discussed in the following sub-sections, taking each latitude sector in turn.

a) Tropics

First, consider the potential predictability of precipitation. The highest values of $\hat{\rho}$, up to 95%, are attained close to the equator in the Pacific and Atlantic Oceans, where convective activity seems most influenced by anomalous SST patterns. Over the equatorial Pacific, the annual cycle of ρ may be partly linked to the typical evolution of SST anomalies during ENSO events. This is seen firstly in the eastern equatorial Pacific close to the South American coast, where there is both a decline of SST anomalies from MAM to DJF during a typical El Nino year (Rasmusson and Carpenter, 1982), and a concurrent fall of (average) predictability (Fig.3). Second, in the west-central equatorial Pacific (160°W to 180°W), there is

a tendency for both El Nino SST anomalies and predictability to rise through the year. This relationship with ENSO is explained by simply presuming that the largest SST anomalies have the greatest impact on local convection, relative to chaos. Over the tropical Atlantic, predictability is also high (despite a lower variance of local SSTs; eg. Bottomley et al., 1990), and exhibits a marked annual cycle with a minimum in SON. This seasonal variation of predictability is supported by an intercomparison with ANOVA estimates from other models (Zwiers et al., 1995), and although its cause is not clear, it seems probable that seasonal variations in the influence of non-local forcings may be important (eg. those from the Pacific; Curtis and Hastenrath, 1995). Over the Indian Ocean, predictability of seasonal rainfall is somewhat lower, and it is suggested that this may be due to the presence of the Madden-Julian Oscillation (MJO) (reviewed by Madden and Julian, 1994) whose amplitude peaks at these longitudes (cf. Goswami, 1993 and Palmer, 1993b, 1994, who consider predictability over India). The relevance of large amplitude low-frequency (intraseasonal) oscillations is that they would effectively reduce the sampling of phase space in each season, causing seasonal means to be more subject to random chaotic variability.

It is over land that predictability of seasonal precipitation is of greatest societal importance, and according to the model the most promising areas include large parts of northern South America, Central America in DJF and SON, parts of coastal Africa, and the Indonesian archipelago. Beginning with South America, the model's predictability corresponds well with the empirical and seasonal forecasting studies for the Nordeste region of Brazil (eg. Ward and Folland, 1991; Hastenrath and Greischar, 1993) (also, Potts et al. (1996) show HADAM1 has high interannual skill here), for Guyana (Hastenrath, 1990), and for Peru and Ecuador (eg. Rasmusson and Carpenter, 1982; Aceituno, 1988), and enables these studies to be put into the wider context of South America's geographical and seasonal variations of predictability. Further north, over the Caribbean and Central America, geographically- and seasonally-dependent predictability also seems possible, with ρ often exceeding 50%. A more in-depth study of this region is clearly warranted, with the competing influences of Pacific (Ropelweski and Halpert, 1987, 1989; Kiladis and Diaz, 1989) and Atlantic (Hastenrath, 1976, 1984) SSTs presumably being of greatest importance. Over Africa, values of ρ are more disappointing. This is especially so during the North African summer (away from the coast), in contrast to Rowell et al. (1995) who found values of $\hat{\rho}$ of 60 to 75% at individual grid points, using a different model. Although their result may be a slight overestimate because of a bias towards extreme years (Rowell, 1996), it is also known that HADAM1's SST-response over the Sahel is particularly poor (noted by Rowell et al., and also Sud and Lau, 1996), and it is expected that a more realistic model would exhibit somewhat larger $\hat{\rho}$ values than those seen in Fig.3 (see further discussion by Rowell, 1996). Over East Africa, the minimum of model predictability occurs in MAM, corresponding with observational studies, eg. Ogallo (1988), Beltrando (1990) and Rowell et al. (1994). The expected peak values for SON are not however attained, and this may be partly because many of the observational studies have analysed regions smaller than the resolution of the model (eg. Farmer, 1988; Ogallo, 1988; Hastenrath et al., 1993). Over southern Africa, the model again fails to attain the amplitude of predictability expected from statistical studies (eg. Hirst and Hastenrath, 1983; Nicholson and Entekhabi, 1987; Lindesay and Vogel, 1990; Walker, 1990). Over the Indonesian archipelago however, results are particularly optimistic for seasonal prediction, especially during the early wet season, SON. This broadly reflects the seasonality of ENSO's influence on rainfall in this region (Ropelweski and Halpert, 1987, 1989; Kiladis and Diaz, 1989), and also the statistical prediction studies of Nicholls (1981) and Hastenrath (1987). Further south however, predictability over Australia is less than expected, given the strong

empirical relationships with SSTs and the SOI (eg. McBride and Nicholls, 1983; Ropelweski and Halpert, 1987, 1989; Nicholls, 1989; Drosdowsky, 1993), and their ongoing use in operational seasonal prediction (M.Voice, personal communication, 1996). The wet-season of the remaining tropical land region, Southeast Asia, is thought by Brankovic and Palmer (1996) to be less predictable than many other tropical regions, probably because of the influence of the MJO mentioned earlier; this is supported by the low ρ values in Fig.3c.

For MSLP, the spatial and seasonal patterns of ρ (Fig.4) have many interesting differences from those for precipitation. Most striking is the larger latitudinal range of high MSLP predictability, reflecting the larger spatial coherence of MSLP and the impact of *random* isolated showers on rainfall totals in the arid sub-tropics. Differences between the annual cycle of ρ for MSLP and precipitation include a JJA minima for MSLP over the Indian and West Pacific oceans not seen for precipitation, and a MAM minima of ρ for West Pacific precipitation not seen for MSLP; reasons for these are not immediately obvious.

b) Mid-Latitudes

In the extratropics, we focus attention mainly on MSLP (Fig.4), which seems more responsive to SSTs than precipitation. In the northern hemisphere, most locations have their highest predictability during winter or spring; from 40° to 60°N the fractional areas where $\hat{\rho}$ exceeds 20%, are 25%, 17%, 13% and 4% for DJF, MAM, JJA and SON, respectively. It seems likely that this is related to higher gradients of potential-vorticity, allowing Rossby waves to communicate predictable signals from the tropics to the extratropics (Brankovic et al., 1994; Palmer and Anderson, 1994). This seasonal peak is particularly apparent over the United States, where values in excess of 40% are achieved along the west coast and over Florida in winter, and over the northwest in spring. In the summer, high predictability is also seen in some southern states, but autumn predictability is low over the entire mid-latitude continent. These variations compare well with observational studies, including the ENSO composites of Ropelweski and Halpert (1987, 1989) and Kiladis and Diaz (1989), and the canonical correlation analysis using global SSTs of Barnston (1994).

Over Europe, the potential for seasonal predictability seems lower than over the United States, and this is probably partly because of a weaker impact of ENSO (Ropelweski and Halpert, 1987, 1989; Kiladis and Diaz, 1989; Fraedrich and Muller, 1992; Fraedrich, 1994). It also explains the less rapid development of operational seasonal forecasting. Potential predictability in winter, spring and summer seem approximately equal over Europe, and are all higher than during autumn (note however, that with error margins of ± 5 to 10% (Fig.1), it is possible that a more pronounced annual cycle of predictability may be hidden by sampling errors). Hence for Europe, it seems that anomalous seasons are primarily the result of chaos, although a notable influence of SSTs, and perhaps pre-season land surface anomalies (eg. Ratcliffe, 1976), cannot be ruled out in occasional years.

Over much of Asia, north of 30°N, the potential for seasonal forecasting suggested by the model is also low. Of the two main exceptions, one is precipitation over southwest Asia during spring and summer, where $\hat{\rho}$ exceeds 30%. Over Japan, predictability of winter precipitation also appears high, and although observations show that winter temperatures may be linked to tropical SSTs and convection (Miyazaki, 1989, 1992), there is no evidence for predictability of precipitation either in the published literature or in the experience of long-range forecasters (M.Sugi, personal communication, 1995); this

particular aspect of Fig.3 is therefore probably erroneous.

In southern hemisphere mid-latitudes, predictability is moderate in all seasons. Regions where $\hat{\rho}$ for MSLP exceeds 30% are as follows. In spring (SON), predictability reaches almost 50% around 60°S 135°W, and this relates well to the pattern of MSLP anomalies arising from decadal variations of the semiannual oscillation (Hurrell and Van Loon, 1994). In winter (JJA), high predictability south of western Australia seems to match the ENSO response described by Karoly (1989) (although his results did not achieve significance here, this may be because of a limited sample of just 3 events). In summer (DJF) however, peaks of predictability seen around 55°S 55°E and 60°S 80°W may have causes other than ENSO, as they do not relate well to Karoly's composite, but correspond better to the wider predictability results of Trenberth (1985) (using the first of the predictability methods described in sect.1).

c) High Latitudes

Poleward of about 60°N/S, a marked annual cycle of predictability is apparent in both hemispheres, where oceanic forcing affects interannual variability of MSLP only in spring, ie. MAM in the northern hemisphere, SON in the southern hemisphere. One explanation may be that this is due to enhanced tropical-extratropical teleconnections, since during spring potential-vorticity gradients are stronger than in summer but internal variability is weaker than in winter (Brankovic et al., 1994; Palmer and Anderson, 1994). This tropical link is supported by performing ANOVA on only the 20 most extreme SOI years (warm and cold events) when tropical forcing is probably strongest, in which case the high latitude aspects of Fig.4 are enhanced (not shown), whereas if only weak and neutral SOI years are used, no spring predictability is found at high latitudes.

Although these experiments do not allow a separate examination of the influence of sea-ice anomalies, it seems that their effects may sometimes be apparent in the smaller scale variables, such as surface air temperature (not shown) or precipitation (Fig.3). The most striking example is over the Barents Sea in winter, where snowfall appears to respond strongly to the (ice/water) state of the sea surface. This particular feature is also apparent in the all-season results of the CSIRO model (Dix and Hunt, 1995, their Fig.5a). The effects of ice-edge variability on large-scale fields such as MSLP are of course almost impossible to distinguish, although the discussion above does suggest that this is negligible in at least most years and seasons. The view that ice-extents sometimes influence local weather but rarely influence the large-scale flow is supported by the synthesis and review of Walsh (1993). A more conclusive finding would only be possible from an ensemble of simulations where the sole forcing is realistic variations of ice-extent.

5. How does the Temporal and Spatial Scale of Analysis affect Seasonal Chaos?

A key issue when applying the above results to seasonal forecasting, is an understanding of the extent to which regional values of ρ are affected by considering smaller or larger space-scales, or shorter or longer time-scales. The desired spatial-temporal resolution of a seasonal forecast is of course highly dependent upon its application. For example, at one extreme, an individual farmer requires information for only a very small area and with as much temporal detail as possible (perhaps including typical lengths of dry spells, etc.); whereas at the other extreme, a management authority for a large river system may need only monthly or seasonal rainfall totals over a substantial area.

As a simple illustration of the dependency of predictability on *temporal*-averaging, consider the Southern Oscillation Index (SOI). Although this hemispheric see-saw of mass responds primarily to SSTs, the effects of chaotic variations are still manifest in its time series. The frequency-dependent nature of the balance between these competing influences is illustrated in Fig.5 (solid line); here the model SOI time series have been filtered using running means of 1 to 24 months, and then the fraction of forced variance computed for each of these filtered ensembles. At a monthly time-scale, the impact of transient disturbances and other chaotic internal modes is quite substantial, accounting for about one third of the SOI's variability. However, as the length of the averaging period increases, the amplitude of the random chaotic variations is reduced, but that of oceanic forcing remains strong (hence ρ increases). For 5-month running means, as typically used when monitoring the SOI (eg. Ropelewski and Jones, 1987; Climate Diagnostics Bulletins, NOAA/NWS/NMC), SST forcing accounts for 86% of the variability. Predictability continues to increase, and reaches a peak of 92% at 18-month running means, before beginning a slow decline. This (perhaps unexpected) fall-off of ρ simply reflects the spectrum of the 'forced component' of variability (μ_i, equation 1); when this has a dominant frequency close to that of the averaging period, then its variance (σ^2_{SST}) is particularly reduced, and for a sufficiently large spectral peak this reduction may exceed the reduction in variance of the random components (simply the inverse of the averaging period), and hence ρ decreases (cf. Trenberth, 1984). It is because (the forced component of) the SOI is dominated by time-scales of two years or more (eg. Trenberth, 1976; Chen, 1982), that the relative impact of SSTs gradually decreases from near this point.

Also shown on Fig.5 (dashed line), as a function of the length of the running mean, is the mean of correlations between an observed SOI time series (using MSLP data provided by P.D.Jones, personal communication, 1993) and each of the six model time series. Following sect.2e, if a perfect model were available, then these mean correlations would be expected to match the ρ values (solid line on Fig.5). In this light, the actual comparison of the two curves indicates the model to be highly skilful in its SOI simulation (although this is perhaps a rather basic test of the model's interannual skill), and also lends support to the frequency-dependent evolution of ρ, as discussed above. Further justification of these results is also obtained by comparison with Trenberth (1984), who analysed "signal-to-noise ratios" using only observed MSLP data. If his ratios are taken as estimates of the quantity $\sigma_{SST}/\sigma_{INT}$, then they can be converted to ρ values using equations 8 and 10. Thus for 1-, 3-, and 12-month means, Trenberth obtains $\hat{\rho}$=67%, 79% and 90%, respectively, compared to $\hat{\rho}$=64%, 81% and 91% from Fig.5. This close match is remarkable, given the use of two quite different analysis techniques and inevitably their quite different underlying assumptions[1].

Returning to a seasonal forecasting perspective, the principles established above are also applicable to the process of averaging months together to form a seasonal mean. In general, the longer the averaging period, the smaller the fraction of variance explained by random chaotic events. However, if the months

[1] Note also that the normalisation procedure used by Trenberth differs from that used here, although he notes that this has only a marginal effect on the signal-to-noise ratio. The index used here was the so-called "Troup" index, ie. Darwin MSLP minus Tahiti MSLP, then normalised with respect to monthly 1951-80 means and standard deviations (cf. Chen, 1982; McBride and Nicholls, 1983; Ropelewski and Jones, 1987).

within a season have a tendency to respond oppositely to SST forcing, then the seasonal mean will be less predictable than (some of) its constituent months.

Likewise, the same principles also apply to the effects of *spatial* averaging on predictability. In general, the larger the area for which a seasonal forecast is required, the more accurate it is likely to be; for example, Rowell et al. (1995) demonstrate that when July to September rainfall is averaged over the entire Sahel (28 grid-boxes), then $\hat{\rho}=96\%$, whereas for individual grid-boxes, the average $\hat{\rho}$ is 76%. However, following the arguments above, it is also important to realise that when oceanic forcing acts in a roughly opposite sense within different parts of a region, then the predictability of the whole region may be less than in some of its sub-regions. It was the application of these principles that led to the decision to degrade the resolution of the precipitation data prior to computing the predictability shown in Fig.3. Since precipitation has relatively low spatial homogeneity, it is likely to be particularly sensitive to the effects of spatial averaging. The effect on Fig.3 of first averaging the data over groups of four grid-boxes was to increase ρ by an average of 4.5% in the tropics (30°N to 30°S), for example from 35.5% to 40.1% in JJA. At a few locations, increases of more than 10% were recorded, whereas at other locations (8% of the area for which ρ is statistically significant) small decreases of predictability were found.

6. Can Interannual Variations of the Amplitude of Seasonal Chaos be Detected?

The calculations of $\hat{\rho}$ described above provide only an 'overall' assessment of predictability; in reality, there may also be variations of predictive skill from year to year. One way of measuring predictability in an individual year is to use a signal-to-noise ratio, eg. $(\mu_i - \mu)/\sigma_i$, where μ is the long-term mean of all x_{ij}'s and σ_i is the standard deviation across the ensemble of the x_{ij}'s in year i. Interannual variations of predictability can thus arise in two ways: (a) variations in the anomalous amplitude of oceanic forcing $(\mu_i - \mu)$, and (b) predictable variations in the relative amplitude of chaotic anomalies (ie. changes in σ_i due to oceanic forcing). The first of these factors is likely to be important wherever SSTs have some influence on interannual variability; further analysis, however, is probably best performed on a regional basis, after identifying critical SST patterns for each region (cf. Brankovic and Palmer, 1996). The relative importance of factor (b), on the other hand, is unknown. The possibility of its importance is best understood if the atmosphere is viewed as a system in which oceanic forcing alters the residence-probability of attractors which are fixed in phase space (cf. Palmer, 1993a), rather than a system in which ocean fluctuations alter the locations of these attractors (the latter, less appropriate but statistically justifiable, viewpoint was necessarily the basis for ANOVA; equation 1). The former viewpoint more naturally gives rise to year-to-year variations of *intraseasonal* variability, eg. by changes to the probabilities of transition between attractors which differ in their preferred residence-times or their size. This intraseasonal variability would then lead to interannual variations of the spread across the ensemble of seasonal means, and thus to the relative 'robustness' of the seasonal mean response to SSTs. It is the aim of this section to explore whether interannual variations of σ_i^2 can be detected with the model data available here, and to describe a methodology appropriate to this end.

Consider first, the variations of ensemble spread for precipitation. At each grid point, a value of $\hat{\sigma}_i^2$ is computed from the sample of 6 runs for each of the 45 years, and the distribution of these 45 $\hat{\sigma}_i^2$'s is compared with another distribution based on the null hypothesis (NH) that the population variances (σ_i^2) for all years are identical, ie. inequalities of the variance estimates arise only from sampling error. If

variations of ensemble spread are predictable (ie. not just due to sampling error), this will affect their distribution and, if the comparison test is powerful enough, the NH will be rejected. The reference NH distribution is generated from 1000 unbiased sample variances, each of the form:

$$\hat{\sigma}^2 = \sum_{k=1}^{6} x'^2_{r(k)} \qquad (42)$$

where each r(k) represents a random selection from the 270 possible values of:

$$x'_r = x_{ij} - \overline{x}_i , \qquad \text{where } r = 1, ..., Nn \qquad (43)$$

(necessarily, we have again returned to the statistical model of equation 1). To compare the two distributions, thus testing the null hypothesis, Kuiper's test (eg. Stephens, 1965; Press et al., 1992) is used. This is an evolution of the Kolmogorov-Smirnov test (eg. Hoel, 1971; Press et al., 1992), but has the advantage of being equally sensitive across the whole distribution, rather than being mainly sensitive at the median, an important point since we are concerned here with tails of the distributions (the alternative hypothesis is for more extreme (large and small) ensemble spreads than under the null hypothesis).

Fig.6 maps the results of applying this test to precipitation at each grid point (on a degraded 5° by 7.5° grid). Field significance was assessed with a Monte Carlo approach, by first computing a further 45 variance estimates at each grid point, each using 6 random choices of x'_r (equations 42 and 43), then testing these against the NH distributions, and calculating the global fraction over which the null hypothesis was rejected at the 95% level. This was repeated 100 times, and on no occasion, for any season, did the significant global fraction exceed that shown in Fig.6; ie. field significance was achieved at better than the 1% level. It was also confirmed that the reason the null hypothesis was rejected was indeed almost always because of a greater propensity towards extreme ensemble spreads. The next step is to determine the reason for these variations of ensemble spread at certain locations. One explanation is that the zero-bounded nature of precipitation might be of crucial importance, since it would have the effect of relating the amplitude of ensemble spread to the amplitude of the ensemble mean. This would be particularly obvious when σ_{SST} is large relative to the climatological mean, and so one would expect a relationship between σ_{SST} / μ and the probabilities shown in Fig.6. This is confirmed by Table 2. The lack of a one-to-one relationship is presumably partly due to erroneous test results because of small ensemble size.

For MSLP, the assessment of ensemble spreads is less clear. Using Kuiper's test, the null hypothesis was rejected at the 95% level over about 4% of the globe in each season, which was not field significant. In an attempt to confirm this result, Bartlett's parametric test for equality of variances (eg. Snedecor and Cochran, 1967; Pearson and Hartley, 1976) was also applied, but with the finding that the same null hypothesis of equal variances was rejected over 9 to 16% of the globe, and that this was field significant at better than the 1% level. Bartlett's test thus seems more powerful than Kuiper's test. However, further investigation of areas of unequal variance was hampered by the co-existence of areas where the null hypothesis was erroneously rejected due to small positive kurtosis, to which Bartlett's test is particularly sensitive; the sample size was too small to allow these areas to be properly demarcated. (Note however, that this occasional small kurtosis of MSLP would have little effect on the F tests used in sect.4; Scheffe, 1959.)

In summary, with 6 realisations of 45 years each, it is only just possible to detect significant interannual variations of ensemble spread. However, as larger ensembles become available, it is anticipated

that such variations will become easier to detect, and their importance and causes can then be further explored.

7. Conclusions and Discussion

The potential skill of seasonal forecasts in a particular region depends primarily on the balance between oceanic forcing and the random effects of chaos. These define predictable and unpredictable components, respectively, which have been separated here by applying 'analysis of variance' (ANOVA) to data from a 6-member 45-year ensemble of simulations with a state-of-the-art climate model. This leads to a worldwide assessment of potential seasonal predictability, described region by region, in the four 'standard' seasons. Sampling error is low (sect.2d), owing to the length and number of simulations, and some of the more doubtful assumptions required by other techniques are superfluous (sect.1).

However, a number of assumptions are still required, two of which are particularly important. First, the assessment depends on the skill of the model's representation of real climate variations. This includes its local response to SST anomalies, regional and planetary-scale teleconnections, and regional responses to these teleconnections. This has been addressed by assessing the model's mean climate and by comparing the magnitude of predictability estimates with observed climate and prediction studies. Further verification is needed on a regional basis (cf. Rowell, 1996), including comparisons with observed data and with predictability estimates from other state-of-the-art models.

The second key assumption of the approach used here, is that potential for seasonal predictability is derived entirely from ocean surface anomalies. This should lead to a good first order estimate of predictability, but further experimentation is required to assess the importance of sources neglected here. Three of these can be highlighted. (a) Pre-season land surface anomalies; these may play a role in maintaining summer droughts for example (eg. Ratcliffe, 1976; Trenberth and Branstator, 1992), and their importance could be tested either with land-surface-forced multi-decadal ensemble experiments (suggested in sect.3a), or with seasonal hindcast experiments set up to compare the impact of (say) realistic versus climatological initial soil moisture distribution. (b) Anthropogenically and naturally induced changes to atmospheric constituents; ideally these should be correctly specified in predictive-GCMs, since they have probably already had a small effect on climate (Mitchell et al., 1995; Santer et al., 1995, 1996; Hegerl et al., 1996), and hence on seasonal anomalies. They may also alter the patterns of predictability in the next few decades, although the nature of such changes will remain unknown unless reliable estimates of the future statistics of SST variations become available. (c) The pre-season atmospheric state; the importance of this is a matter of debate, centring on whether chaotic atmospheric anomalies can persist for a season or more without external forcing (eg. Shukla, 1985; James and James, 1989), or whether the seasonal solar cycle prevents such persistence (Lorenz, 1990); this is unlikely to be a major factor, but also requires investigation.

The results of the potential predictability maps displayed in this paper may be summarised as follows. Predictability is not surprisingly highest in the tropics, where the influence of chaos is relatively small. However, substantial longitudinal variations of tropical predictability are also found, for some of which the influence of chaos is substantial. Encouragingly, smaller but consistent influences of oceanic forcing are found for many mid-latitude regions. The well-known seasonal predictability over parts of North America is supported, and hope is also provided that lower-skill forecasts may be possible over parts

of Europe and mid-latitude Asia. In high latitudes, MSLP in spring has a small but discernable influence from tropical SSTs, but is entirely chaotic in other seasons. High-latitude precipitation, on the other hand, can experience a moderate influence of the local sea state close to ice-edges in some regions. In general, the predictability maps seem realistic on a global scale, and usually plausible on a regional scale, thus enabling many locally-focused observational studies to be placed in a regional context. However, some model problems were inevitably revealed, particularly where oceanic forcing seemed erroneously weak.

A more complete and practically focused study of seasonal predictability requires a more extensive analysis than that presented here. First, 'non-standard' seasonal definitions of varying length should be included. In sect.5, it was shown how predictability is usually enhanced by temporal (or spatial) averaging, although, counter-intuitively, it is also reduced in certain circumstances. Application of ANOVA to other variables is also needed, including seasonal means of other parameters (eg. temperature, height, etc.), higher moment seasonal statistics (eg. intraseasonal variance), EOF time coefficients, and count-data such as blocking frequency (for which an adaptation of ANOVA would be needed; Zwiers, personal communication, 1995). (See also Zwiers et al., 1995, for further suggestions on the application of ANOVA.) These analyses will also be invaluable from the perspective of simply understanding climate variability.

Another practical issue is the likelihood of year-to-year variations of predictability. If years of high or low predictability could be determined in advance, this would be very useful. There are two factors to consider. One is variations in the anomalous amplitude of oceanic forcing, which are probably best assessed on a regional basis. The other is year-to-year variations in the seasonal mean *amplitude* of chaotic variations, which if affected by oceanic forcing would be partly predictable. An initial analysis was presented in sect.6, and it was concluded that although some effect could just be detected, statistical sampling was a major problem with only 6 runs; a more useful assessment of this effect must await larger ensembles.

Finally, perhaps the most interesting avenue for further research, is to understand the mechanisms by which ocean surface anomalies affect seasonal variability. Many questions are raised by the analysis presented here, particularly including speculation of the reasons for spatial and seasonal variations of predictability. Simulation data, such as that utilised here, provides excellent material to pursue these questions.

Acknowledgements. The advice of John Rowell has been much appreciated, and also discussions with Chris Folland, Gil Ross, Masato Sugi and Francis Zwiers. Thanks is due to David Sexton, Alison Renshaw and John Davies for running the model and developing some of the software. Computer time was provided by the UK Department of Environment, under contract PECD7/12/37, with further partial support under CEC contract EV5V-CT92-0121 ("Medium Term Climate Variability"). Gridded observed MSLP data was kindly provided by Tracy Basnett and David Parker, gridded rainfall data (GU23WLD0094.DAT) was constructed by Mike Hulme at the Climatic Research Unit, Norwich, under UK DoE contract PECD7/12/78, and Tahiti and Darwin MSLP data was supplied by Phil Jones.

REFERENCES

Aceituno, P., 1988: On the functioning of the southern oscillation in the South American sector. Part I: Surface climate. Mon. Wea. Rev., 116, 505-524

Barnston, A.G., 1994: Linear statistical short-term climate predictive skill in the northern hemisphere. J. Climate, 7, 1513-1564

Barnston, A.G., van den Dool, H.M., Zebiak, S.E., Barnett, T.P., Ji, M., Rodenhuis, D.R., Cane, M.A., Leetmaa, A., Graham, N.E., Ropelewski, C.R., Kousky, V.E., O'Lenic, E.A. and Livezey, R., 1994: Long-lead seasonal forecasts - where do we stand? Bull. Amer. Meteor. Soc., 75, 2097-2114

Basnett, T.A. and Parker, D.E., 1995: Provisional new global mean sea level pressure data set. In: "Workshop on Simulations of the Climate of the Twentieth Century using GISST, 28-30 November 1994, Hadley Centre, Bracknell, UK", Folland, C.K. and Rowell, D.P. (Eds), Climate Research Technical Note No.56 (unpublished document available from the Hadley Centre, UK Meteorological Office, Bracknell), 58-59

Beltrando, G., 1990: Space-time variability of rainfall in April and October-November over East Africa during the period 1932-1983. Int. J. Climatol.,10, 691-702

Bottomley, M., Folland, C.K., Hsiung, J., Newell, R.E. and Parker, D.E., 1990: Global Ocean Surface Temperature Atlas. Joint Met. Office/MIT Project, 20pp. + 313 plates, funded by UK Depts. of Energy and Environment, HMSO, London

Brankovic, C. and Palmer, T.N., 1996: Atmospheric seasonal predictability and estimates of ensemble size. Mon. Wea. Rev., submitted

Brankovic, C., Palmer, T.N. and Ferranti, L., 1994: Predictability of seasonal atmospheric variations. J. Climate, 7, 217-237

Cane, M.A., Zebiak, S.E. and Dolan, S.C., 1986: Experimental forecasts of El Nino. Nature, 321, 827-832

Charney, J.G. and Shukla, J., 1981: Predictability of monsoons. In: "Monsoon Dynamics", Lighthill, J. and Pearce, R.P. (Eds.), Cambridge Univ. Press., 99-109

Chen, W.Y., 1982: Assessment of Southern Oscillation sea-level pressure indices. Mon. Wea. Rev., 110, 800-807

Chervin, R.M., 1988: Predictability of time-averaged atmospheric states. In: Physically-Based Modelling and Simulation of Climate and Climate Change - Part II, Schlesinger, M.E. (Ed.), Kluwer Academic Publishers, 983-1008

Cullen, M.J.P, 1993: The unified forecast/climate model. Meteor. Mag., 122, 81-94

Curtis, S. and Hastenrath, S., 1995: Forcing of anomalous sea surface temperature evolution in the tropical Atlantic during Pacific warm events. J. Geophys. Res., 100, C8, 15835-15847

Dix, M.R. and Hunt, B.G., 1995: Chaotic influences and the problem of deterministic seasonal predictions. Int. J. Climatol., 15, 729-752

Donoghue, J.R. and Collins, L.M., 1990: A note on the unbiased estimate of the intraclass correlation. Psychometrika, 55, 159-164

Drosdowsky, W., 1993: An analysis of Australian seasonal rainfall anomalies: 1950-1987. II: Temporal variability and teleconnection patterns. Int, J. Climatol., 13, 111-149

Farmer, G., 1988: Seasonal forecasting of the Kenya Short Rains, 1901-84. J. Climatol., 8, 489-497

Fiorino, M., 1995: AMIP overview - analysis of the base state. WMO/WCRP 92, Proceedings of the First International AMIP Scientific Conference, Monterey, Calif., 15-19 May 1995, 9-11

Fraedrich, K., 1994: An ENSO impact on Europe? A review. Tellus, 46A, 541-552

Fraedrich, K. and Muller, K., 1992: Climate anomalies in Europe associated with ENSO extremes. Int. J. Climatol., 12, 25-31

Frederiksen, C.S., Bevan, A., Navarra, A., Hoerling, M., Miyakoda, M. and Ward, M.N., 1995: AGCM intercomparison diagnostics: Climatologies and ENSO teleconnections (1951-80). In: "Workshop on Simulations of the Climate of the Twentieth Century using GISST, 28-30 November 1994, Hadley Centre, Bracknell, UK", Folland, C.K. and Rowell, D.P. (Eds), Climate Research Technical Note No.56 (unpublished document available from the Hadley Centre, UK Meteorological Office, Bracknell), 14-34

Gates, W.L., 1992: AMIP: The atmospheric model intercomparison project. Bull. Amer. Meteor. Soc., 73, 1962-1970

Gates, W.L., Henderson-Sellers, A., Boer, G.J., Folland, C.K., Kitoh, A., McAvaney, B., Semazzi, F., Smith, N., Weaver, A.J., and Zeng, Q.-C., 1995: Climate models - evaluation. In: "Climate Change 1995: The Science of Climate Change. The Second Assessment Report of the Intergovernmental Panel on Climate Change: Contribution to Working Group I." Houghton, J.J., Meira Filho, L.G., Callander, B.A., Harris, N., Kattenberg, A. and Maskell, K. (Eds.). Cambridge University Press, Cambridge, UK., in press

Goswami, B.N., 1993: Difficulties in simulation of time mean monsoon circulation: some thoughts. WMO/WCRP 80, Simulation and Prediction of Monsoons: Recent Results, 27-32

Harzallah, A. and Sadourny, R., 1995: Internal versus SST-forced atmospheric variability as simulated by an atmospheric general circulation model. J.Climate, 8, 474-495

Hastenrath, S., 1976: Variations in low-latitude circulation and extreme climatic events in the tropical Americas. J. Atmos. Sci., 33, 202-215

Hastenrath, S., 1984: Interannual variability and annual cycle: mechanisms of circulation and climate in the tropical Atlantic sector. Mon. Wea. Rev., 112, 1097-1107

Hastenrath, S., 1987: Predictability of Java monsoon rainfall anomalies: a case study. J. Climate Appl. Meteor., 26, 133-141

Hastenrath, S., 1990: Predictability of anomalous river discharge in Guyana. Nature, 345, 53-54

Hastenrath, S. and Greischar, L., 1993: Further work on the prediction of Northeast Brazil rainfall anomalies. J. Climate, 6, 743-758

Hastenrath, S., Nicklis, A. and Greischar, L., 1993: Atmospheric-hydrospheric mechanisms of climate anomalies in the Western Equatorial Indian Ocean. J. Geophys. Res., 98, C11, 20219-20235

Hegerl, G.C., von Storch, H., Hasselmann, K., Santer, B.D., Cubasch, U. and Jones, P.D., 1996: Detecting greenhouse gas induced climate change with an optimal fingerprint method. J. Climate, in press

Hirst, A.C. and Hastenrath, S., 1983: Atmosphere-ocean mechanism of climate anomalies in the Angola - tropical Atlantic sector. J. Phys. Oceanogr., 13, 1146-1157

Hoel, P.G., 1971: Introduction to mathematical statistics. John Wiley, New York, 409pp

Hulme, M., 1994: Validation of large-scale precipitation fields in general circulation models. In: "Global Precipitation and Climate Change", Debois, M. and Desalmand, F. (Eds.), NATO ASI Series, Vol. I 26, Springer-Verlag, Berlin, 387-405

Hurrell, J.W. and Van Loon, H., 1994: A modulation of the atmospheric annual cycle in the southern hemisphere. Tellus, 46A, 325-338

James, I.N. and James, P.M., 1989: Ultra-low-frequency variability in a simple atmospheric circulation model. Nature, 342, 53-55

Ji, M., Kumar, A., Leetmaa, A., 1994: A multiseason climate forecast system at the National Meteorological Centre. Bull. Amer. Meteor. Soc., 75, 569-577

Karoly, D.J., 1989: Southern hemisphere circulation features associated with El Nino - Southern Oscillation events. J. Climate, 2, 1239-1252

Kiladis, G.N. and Diaz, H.F., 1989: Global climatic anomalies associated with extremes in the Southern Oscillation. J. Climate, 2, 1069-1090

Kumar, A. and Hoerling, M.P., 1995: Prospects and limitations of seasonal atmospheric GCM predictions. Bull. Amer. Meteor. Soc., 76, 335-345

Lau, N.-C., 1985: Modeling the seasonal dependence of the atmospheric response to observed El Ninos in 1962-76. Mon. Wea. Rev., 113, 1970-1996

Legates, D.R. and Willmott, C.J., 1990: Mean seasonal and spatial variability in gauge-corrected, global precipitation. Int. J. Climatol., 10, 111-127

Lindesay, J.A. and Vogel, C.H., 1990: Historical evidence for southern oscillation - southern African rainfall relationships. Int. J. Climatol., 10, 679-689

Lorenz, E.N., 1963: Deterministic non-periodic flow. J. Atmos. Sci., 20, 130-141

Lorenz, E.N., 1990: Can chaos and intransitivity lead to interannual variability? Tellus, 42A, 378-389

Lorenz, E.N., 1993: The essence of chaos. University of Washington Press, Seattle, 227pp

Madden, R.A., 1976: Estimates of natural variability of time-averaged sea-level pressure. Mon. Wea. Rev., 104, 942-952

Madden, R.A. and Julian, P.R., 1994: Observations of the 40-50 day tropical oscillation - a review. Mon. Wea. Rev., 122, 814-837

McBride, J.L. and Nicholls, N., 1983: Seasonal relationships between Australian rainfall and the Southern Oscillation. Mon. Wea. Rev., 111, 1998-2004

Mitchell, J.F.B., Johns, T.C., Gregory, J.M. and Tett, S.F.B., 1995: Climate response to increasing levels of greenhouse gases and sulphate aerosols. Nature, 376, 501-504

Miyazaki, Y., 1989: The relationship between tropical convection and winter weather over Japan. J. Meteorol. Soc. Japan, 67, 863-875

Miyazaki, Y., 1992: Relationship between sea-water temperature in the tropics and winter weather in Japan. J. Meteorol. Soc. Japan, 70, 769-774

Nicholls, N., 1981: Air-sea interaction and the possibility of long-range weather prediction in the Indonesian Archipelago, Mon. Wea. Rev., 109, 2435-2443

Nicholls, N., 1989: Sea surface temperatures and Australian winter rainfall. J. Climate, 2, 965-973

Nicholson, S.E., and Entekhabi, D., 1987: Rainfall variability in Equatorial and Southern Africa: Relationships with sea surface temperature along the southwestern coast of Africa. J. Climate Applied Meteor., 26, 561-578.

Ogallo, L.J., 1988: Relationships between seasonal rainfall in East Africa and the Southern Oscillation. Int. J. Climatol., 8, 31-43

Palmer, T.N., 1993a: Extended-range atmospheric prediction and the Lorenz model. Bull. Amer. Meteor. Soc., 74, 49-65

Palmer, T.N., 1993b: Some thoughts on monsoon predictability. WMO/WCRP 80, Simulation and Prediction of Monsoons: Recent Results, 51-57

Palmer, T.N., 1994: Chaos and predictability in forecasting the monsoons. Proc. Indian Natn. Sci. Acad., 60A, 57-66

Palmer, T.N. and Anderson, D.L.T., 1994: The prospects for seasonal forecasting - A review paper. Q. J. R. Meteorol. Soc., 120, 755-793

Parker, D.E., Folland, C.K., Bevan, A., Ward, M.N., Jackson, M., and Maskell, K. 1995: Marine surface data for analyses of climatic fluctuations on interannual to century time scales. In: "Climate Variability on Decade to Century Time scales", US Nat. Acad. Sci, in press

Pearson, E.S. and Hartley, H.O., 1976: Biometrika tables for statisticians. Vol I. University College, London, 270pp

Phillips, T.J., 1994: A summary documentation of the AMIP models. PCMDI Report No.18, Univ. of Calif., Lawrence Livermore National Laboratory, Calif.

Potts, J.M, Folland, C.K., Jolliffe, I.T. and Sexton, D., 1996: Revised "LEPS" scores for assessing climate model simulations and long-range forecasts. J. Climate, 9, 34-53

Press, W.H., Teukolsky, S.A., Vetterling, W.T. and Flannery, B.P., 1992: Numerical recipes in FORTRAN. Cambridge University Press, 963pp

Rasmusson, E.M. and Carpenter, T.H. 1982: Variations in tropical sea surface temperature and surface wind fields associated with the southern oscillation/El Nino. Mon. Wea. Rev., 110, 354-384

Ratcliffe, R.A., 1976: The hot spell of late June-early July 1976. Weather, 31, 355-357

Ropelewski, C.F. and Jones, P.D., 1987: An extension of the Tahiti-Darwin Southern Oscillation index. Mon. Wea. Rev., 115, 2161-2165

Ropelewski, C.F. and Halpert, M.S., 1987: Global and regional scale precipitation patterns associated with the El Nino/Southern Oscillation. Mon. Wea. Rev., 115, 1606-1625

Ropelewski, C.F. and Halpert, M.S., 1989: Precipitation patterns associated with the high index phase of the southern oscillation. J. Climate, 2, 268-284

Rowell, D.P., 1996: Reply to comments by Y.C. Sud and W.K.-M. Lau on 'Variability of summer rainfall over tropical north Africa (1906-92): Observations and modelling' by D.P. Rowell, C.K. Folland, K. Maskell and M.N. Ward (April 4, 1995, 121, 669-704): Further analysis of simulated interdecadal and interannual variability of summer rainfall over tropical north Africa. Q. J. R. Meteorol. Soc., in press

Rowell, D.P., Ininda, J.M. and Ward, M.N., 1994: The Impact of Global Sea Surface Temperature Patterns on Seasonal Rainfall in East Africa. WMO/WCRP 84, Proceedings of the International Conference on Monsoon Variability and Prediction, 666-672

Rowell, D.P., Folland, C.K., Maskell, K. and Ward, M.N., 1995: Variability of Summer Rainfall over Tropical North Africa (1906-92): Observations and Modelling. Q. J. R. Meteorol. Soc., 121, 669-704

Santer, B.D., Wigley, T.M.L., Barnett, T.P. and Anyamba, E., 1995: Detection of climate change and attribution of causes. In: "Climate Change 1995: The Science of Climate Change. The Second Assessment Report of the Intergovernmental Panel on Climate Change: Contribution to Working Group I." Houghton, J.J., Meira Filho, L.G., Callander, B.A., Harris, N., Kattenberg, A. and Maskell, K. (Eds.). Cambridge University Press, Cambridge, UK., in press

Santer, B.D., Taylor, K.E., Wigley, T.M.L., Jones, P.D., Karoly, D.J., Mitchell, J.F.B., Oort, A.H., Penner, J.E., Ramaswamy, M.D., Schwarzkopf, R.J. and Tett, S., 1996: A search for human influences on the thermal structure of the atmosphere. Nature, submitted

Scheffe, H., 1959: The analysis of variance. John Wiley and Sons, New York, 477pp

Shukla, J., 1985: Predictability. Adv. Geophys., 28B, 87-122

Shukla, J. and Gutzler, D.S., 1983: Interannual variability and predictability of 500 mb geopotential heights over the northern hemisphere. Mon. Wea. Rev., 111, 1273-1279

Snedecor, G.W. and Cochran, W.G., 1967: Statistical Methods. Iowa State University Press, Iowa, 593pp

Stephens, M.A., 1965: The goodness-of-fit statistic V_N: distribution and significance points. Biometrika, 52, 309-321

Stern, W. and Miyakoda, K., 1995: The feasibility of seasonal forecasts speculated from multiple GCM simulations. J. Climate, 8, 1071-1085

Sud, Y.C. and Lau, W.K.-M., 1996: Comments on 'Variability of summer rainfall over tropical north Africa (1906-92): Observations and modelling' by D.P. Rowell, C.K. Folland, K. Maskell and M.N. Ward (April 4, 1995, 121, 669-704). Q. J. R. Meteorol. Soc., in press

Trenberth, K.E., 1976: Spatial and temporal variations of the Southern Oscillation. Q. J. R. Meteorol. Soc., 102, 639-653

Trenberth, K.E., 1984: Signal versus noise in the Southern Oscillation. Mon. Wea. Rev., 112, 326-332

Trenberth, K.E., 1985: Potential predictability of geopotential heights over the southern hemisphere. Mon. Wea. Rev., 113, 54-64

Trenberth, K.E. and Branstator, G.W., 1992: Issues in establishing causes of the 1988 drought over North America. J. Climate, 5, 159-172

Walker, N.D., 1990: Links between South African summer rainfall and temperature variability of the Agulhas and Benguela current system. J. Geophys Res., 95, 3297-3319

Walsh, J.E., 1993: Observational and modelling studies of the influence of sea ice anomalies on atmospheric circulation. In: NATO ASI Series, Vol. I6, "Prediction of Interannual Climate Variations", Ed. J.Shukla (Springer-Verlag, Berlin,), 71-88

Ward, M.N. and Folland, C.K., 1991: Prediction of seasonal rainfall in the North Nordeste of Brazil using eigenvectors of sea surface temperatures. Int. J. Climatol., 11, 711-743

Ward, M.N., Folland, C.K., Maskell, K., Colman, A., Rowell, D.P. and Lane, K., 1993: Experimental seasonal forecasting of tropical rainfall at the U.K. Meteorological Office. In: NATO ASI Series, Vol. I6, "Prediction of Interannual Climate Variations", Ed. J.Shukla (Springer-Verlag, Berlin,), 197-216

Warrilow, D.A., Sangster, A.B. and Slingo, A., 1986: Modelling of land surface processes and their influence on European climate. Dyn. Climatol. Tech. Note No. 38 (unpublished document available from the Hadley Centre, UK Meteorological Office, Bracknell)

Willmott, C.J., Rowe, C.M. and Mintz, Y., 1985: A global archive of land cover and soils data for use in general circulation climate models. J. Climatol., 5, 119-143

Zwiers, F.W., 1987: A potential predictability study conducted with an atmospheric general circulation model. Mon. Wea. Rev., 115, 2957-2974

Zwiers, F.W., Rowell, D.P., Hense, A., Davies, J.R. and Christoph, M., 1995: AGCM intercomparison diagnostics: SST-Forced variability versus internal variability. In: "Workshop on Simulations of the Climate of the Twentieth Century using GISST, 28-30 November 1994, Hadley Centre, Bracknell, UK", Folland, C.K. and Rowell, D.P. (Eds), Climate Research Technical Note No.56 (unpublished document available from the Hadley Centre, UK Meteorological Office, Bracknell), 35-39

Table 1 Spatial correlations between observed and simulated 1961-90 climatologies (mean and interannual standard deviation). The area-weighted computations are over 90°N-80°S at a 5° by 5° resolution for MSLP, and over 70°N-60°S at a 5° by 7.5° resolution for precipitation.

Field	Statistic	Verification Data	DJF	MAM	JJA	SON
MSLP	Mean	Basnett-Parker	0.96	0.97	0.97	0.97
MSLP	Stan. dev.	Basnett-Parker	0.90	0.82	0.77	0.74
Precip	Mean	Legates-Willmott	0.65	0.65	0.63	0.66
Precip	Mean	Hulme	0.78	0.67	0.70	0.77
Precip	Stan. dev.	Hulme	0.81	0.75	0.78	0.77

Table 2 Relationship between σ_{SST} / μ for precipitation (1949-93) and the probabilities shown in Fig.6. For each specified range of σ_{SST} / μ, 'No.' is the total number of 5° by 7.5° grid-boxes in this range, and 'Percnt.' is the percentage of these boxes achieving significance at the 5% level in Fig.6.

	$0.0 \le \frac{\sigma_{SST}}{\mu} < 0.1$		$0.1 \le \frac{\sigma_{SST}}{\mu} < 0.2$		$0.2 \le \frac{\sigma_{SST}}{\mu} < 0.3$		$0.3 \le \frac{\sigma_{SST}}{\mu} < 0.4$		$0.4 \le \frac{\sigma_{SST}}{\mu} < 0.5$		$\frac{\sigma_{SST}}{\mu} \ge 0.5$	
Season	No.	Percnt.	No.	Percnt.	No.	Percnt.	No.	Percnt.	No.	Percnt.	No.	Percnt.
DJF	989	4.4	347	7.2	200	18.0	106	27.4	46	54.3	40	67.5
MAM	997	4.1	352	9.9	184	18.5	95	30.5	57	54.4	43	65.1
JJA	1048	5.5	355	13.5	175	19.4	59	30.5	35	40.0	56	76.8
SON	1049	4.4	350	8.6	181	26.0	66	39.4	37	54.1	45	75.6

Figure Captions

Fig.1 Confidence intervals for ρ, for (a) 10-year experiments, and (b) 45-year experiments. Thick line represents the best estimate of ρ. Thin lines, computed for various sized ensembles, define the limits between which the true value of ρ lies with 90% confidence.

Fig.2 1961-90 model climatologies. (a) DJF MSLP; (b) JJA MSLP; (c) DJF precipitation; (d) JJA precipitation. Errors from observed data of greater than 5hPa (MSLP) or 5mm day^{-1} (precipitation) are shown by heavy stippling for positive model errors and light stippling for negative model errors. Note that the observed MSLP data extends only to 80°S.

Fig.3 Percentage variance of seasonal mean precipitation due to oceanic forcing, computed from the ensemble of six 1949-93 runs. Data was first interpolated to a 5° by 7.5° grid. Results for each of four 'standard' seasons are shown. The contour interval is 10%, and white areas show where values do not significantly exceed zero at the 5% significance level (tested using log-precipitation; see sect.2c).

Fig.4 Percentage variance of seasonal mean MSLP due to oceanic forcing, computed from the ensemble of six 1949-93 runs. Results for each of four 'standard' seasons are shown. The contour interval is 10%, and white areas show where values do not significantly exceed zero at the 5% significance level.

Fig.5 Characteristics of the SOI as a function of temporal filtering (using running means from 1 to 24 months). Solid line shows the percentage variance due to oceanic forcing, using the ensemble of six 1949-93 runs. Dashed line shows the mean of correlations (x100) between an observed time series and each of the model time series.

Fig.6 Probability (using Kuiper's test) that yearly cross-ensemble variances of seasonal precipitation (on a 5°x7.5° grid) derive from the same population. Results for each of four 'standard' seasons are shown. At the top of each plot, the fraction of the globe which achieves significance at the 5% level is shown (taking account of the diminishing size of grid-boxes at higher latitudes). See text for further detail.

Fig.1 Confidence intervals for ρ, for (a) 10-year experiments, and (b) 45-year experiments. Thick line represents the best estimate of ρ. Thin lines, computed for various sized ensembles, define the limits between which the true value of ρ lies with 90% confidence.

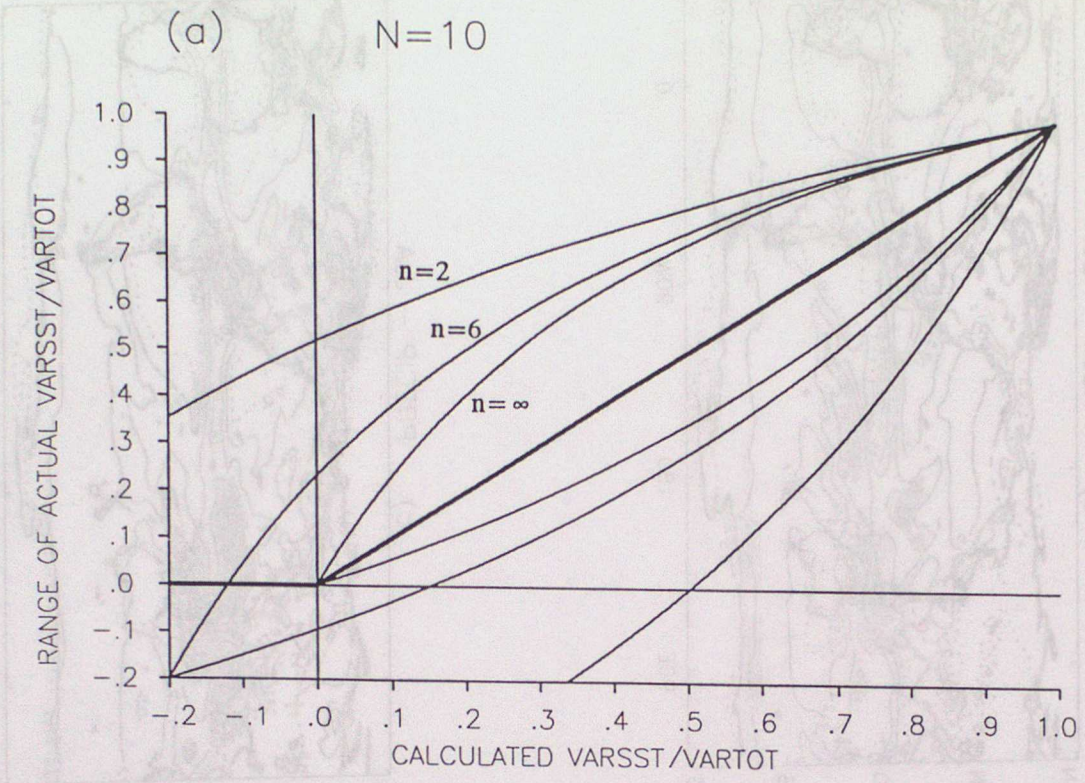

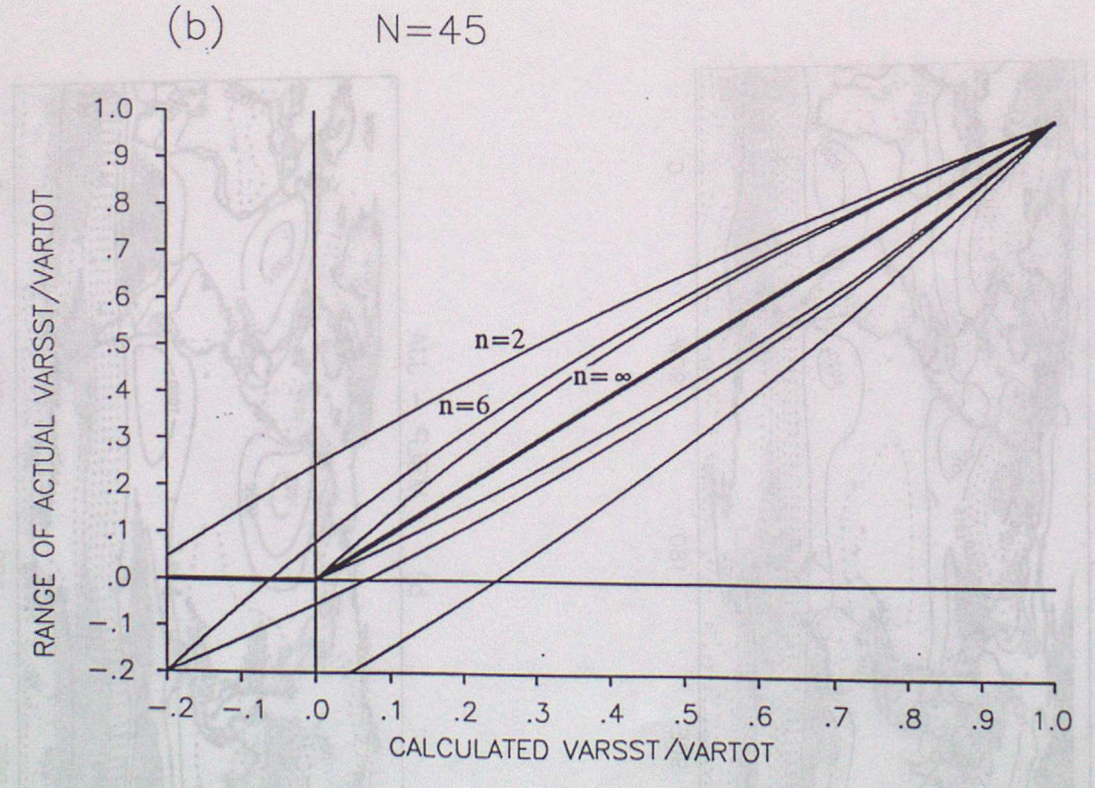

Fig.2 1961-90 model climatologies. (a) DJF MSLP; (b) JJA MSLP; (c) DJF precipitation; (d) JJA precipitation. Errors from observed data of greater than 5hPa (MSLP) or 5mm day^{-1} (precipitation) are shown by heavy stippling for positive model errors and light stippling for negative model errors. Note that the observed MSLP data extends only to 80°S.

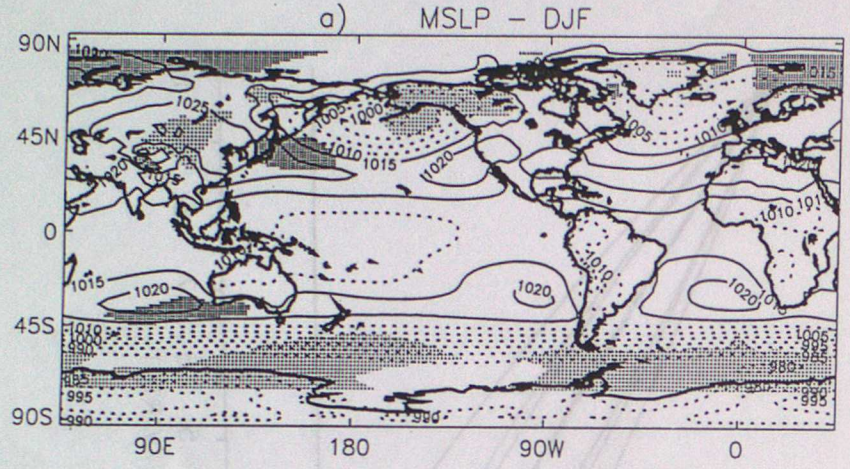

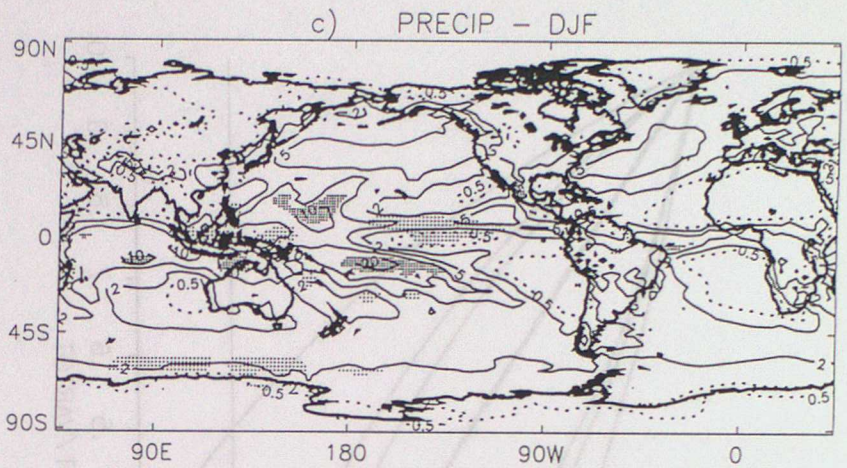

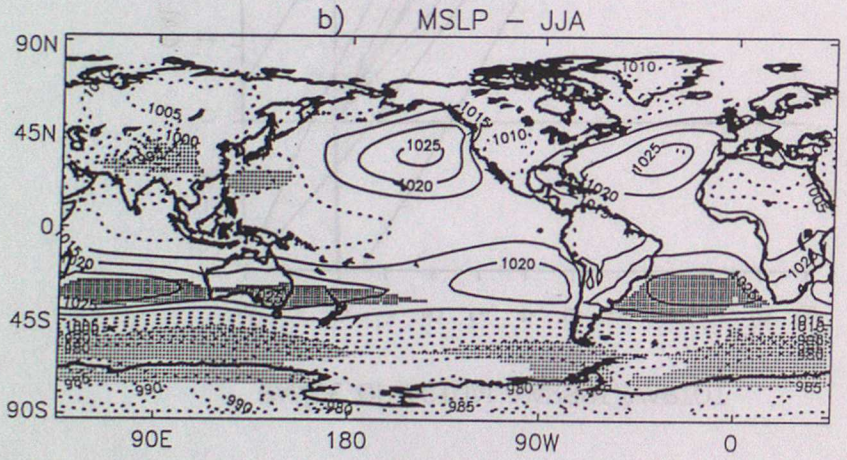

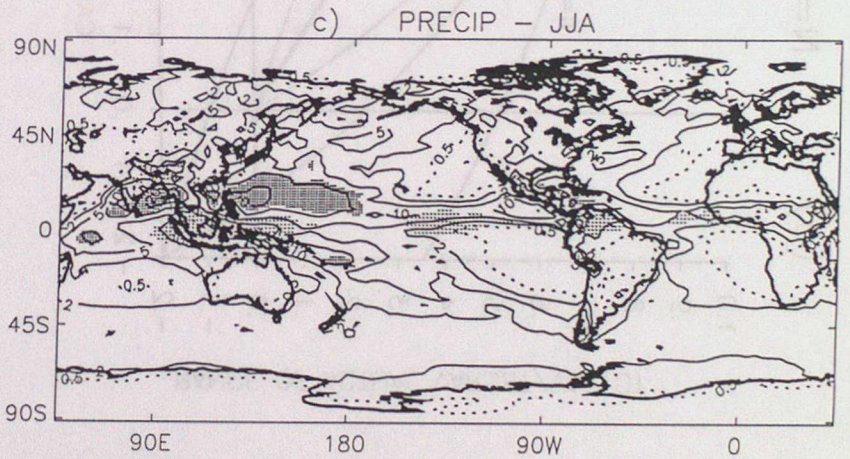

Fig.3 Percentage variance of seasonal mean precipitation due to oceanic forcing, computed from the ensemble of six 1949-93 runs. Data was first interpolated to a 5° by 7.5° grid. Results for each of four 'standard' seasons are shown. The contour interval is 10%, and white areas show where values do not significantly exceed zero at the 5% significance level (tested using log-precipitation; see sect.2c).

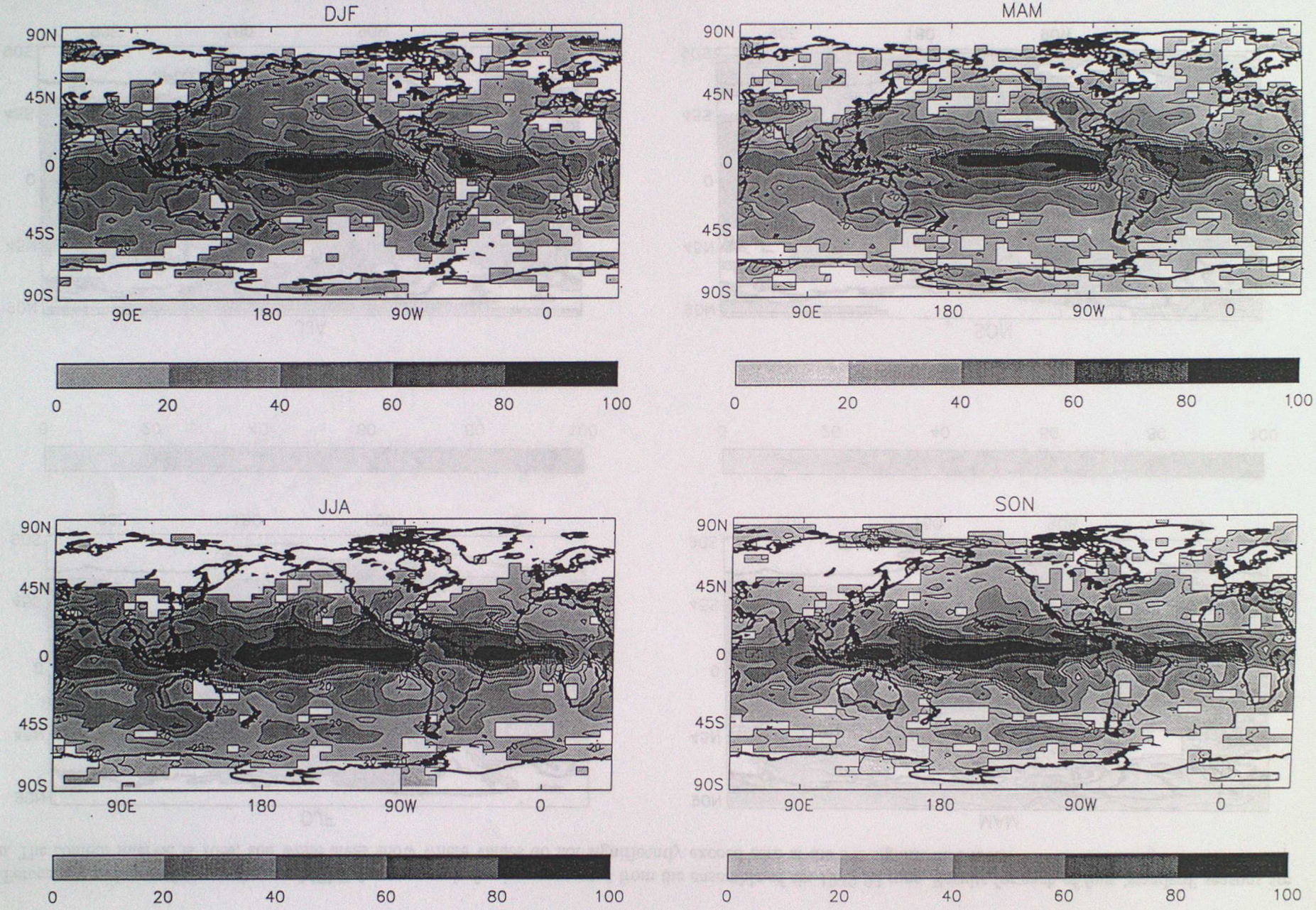

Fig.4 Percentage variance of seasonal mean MSLP due to oceanic forcing, computed from the ensemble of six 1949-93 runs. Results for each of four 'standard' seasons are shown. The contour interval is 10%, and white areas show where values do not significantly exceed zero at the 5% significance level.

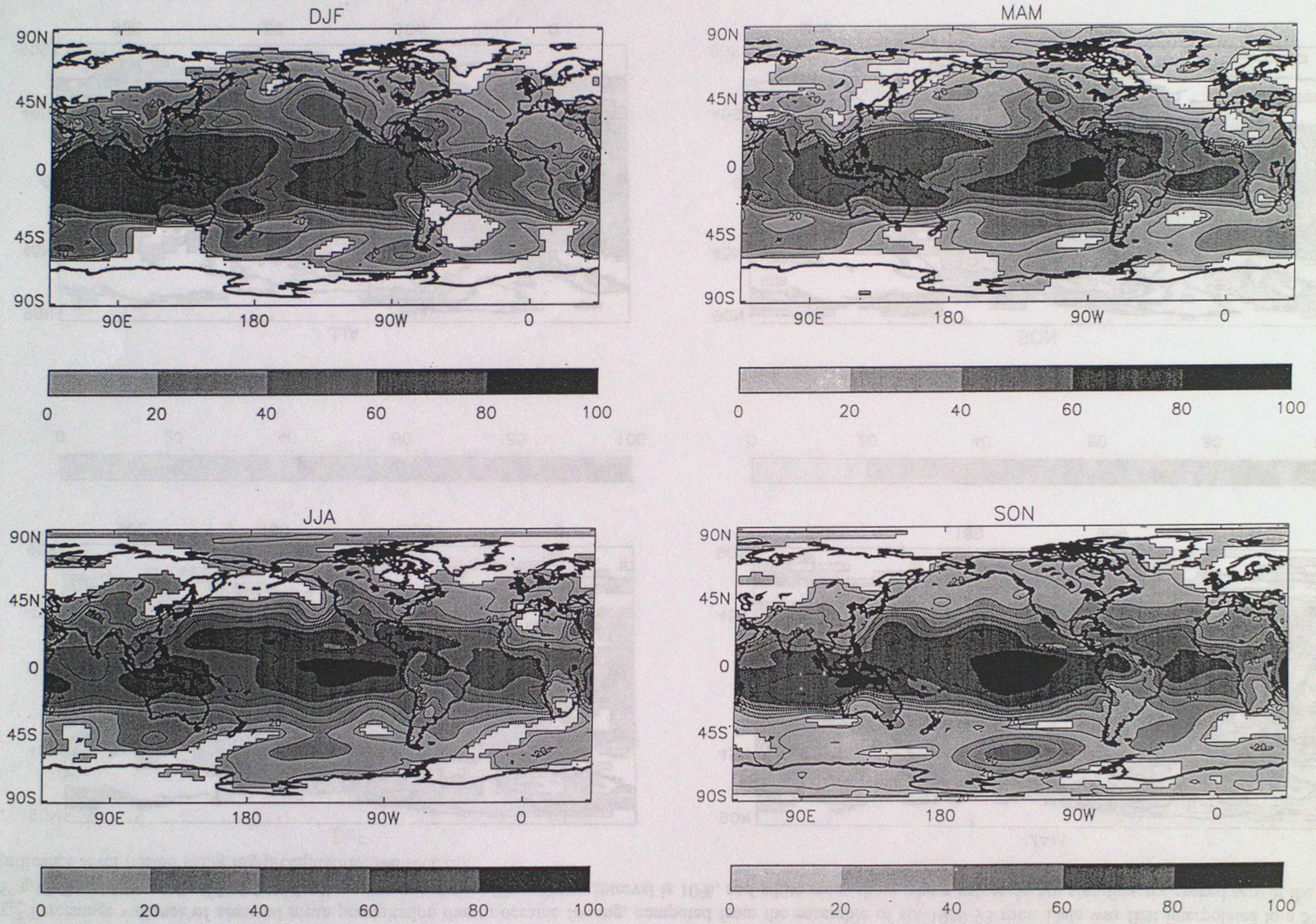

Fig.5 Characteristics of the SOI as a function of temporal filtering (using running means from 1 to 24 months). Solid line shows the percentage variance due to oceanic forcing, using the ensemble of six 1949-93 runs. Dashed line shows the mean of correlations (x100) between an observed time series and each of the model time series.

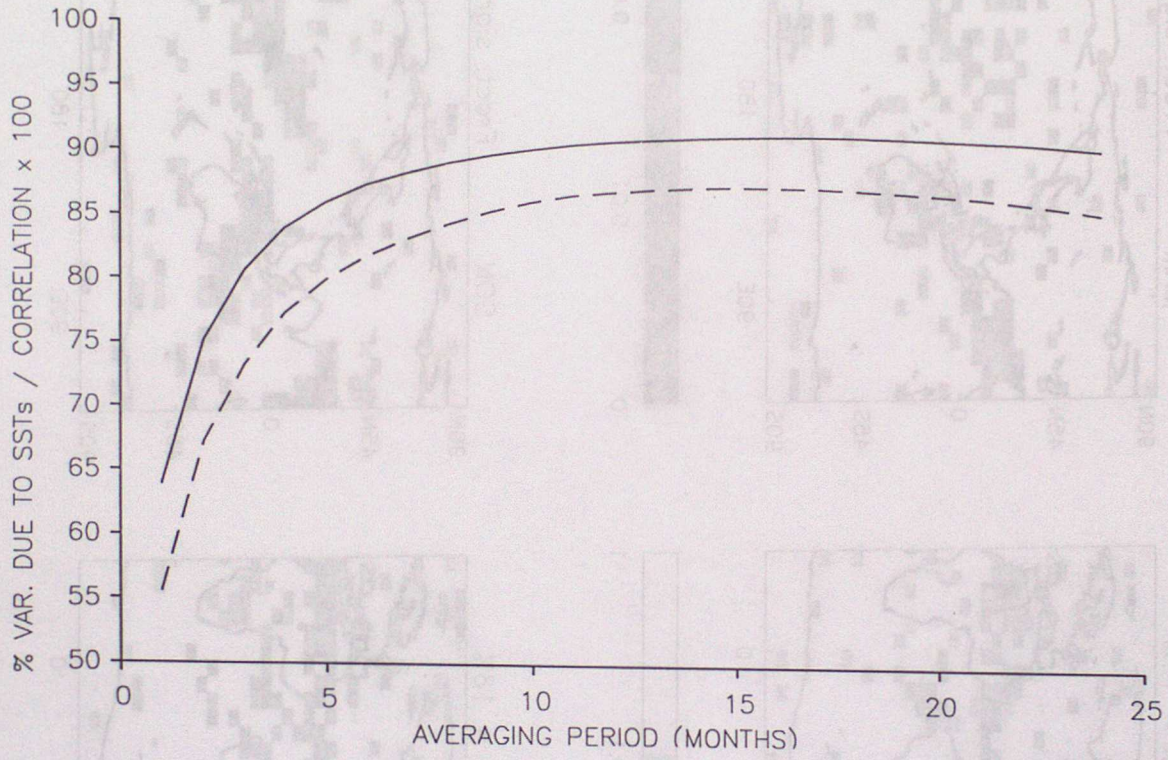

Fig.6 Probability (using Kuiper's test) that yearly cross-ensemble variances of seasonal precipitation (on a 5°x7.5° grid) derive from the same population. Results for each of four 'standard' seasons are shown. At the top of each plot, the fraction of the globe which achieves significance at the 5% level is shown (taking account of the diminishing size of grid-boxes at higher latitudes). See text for further detail.

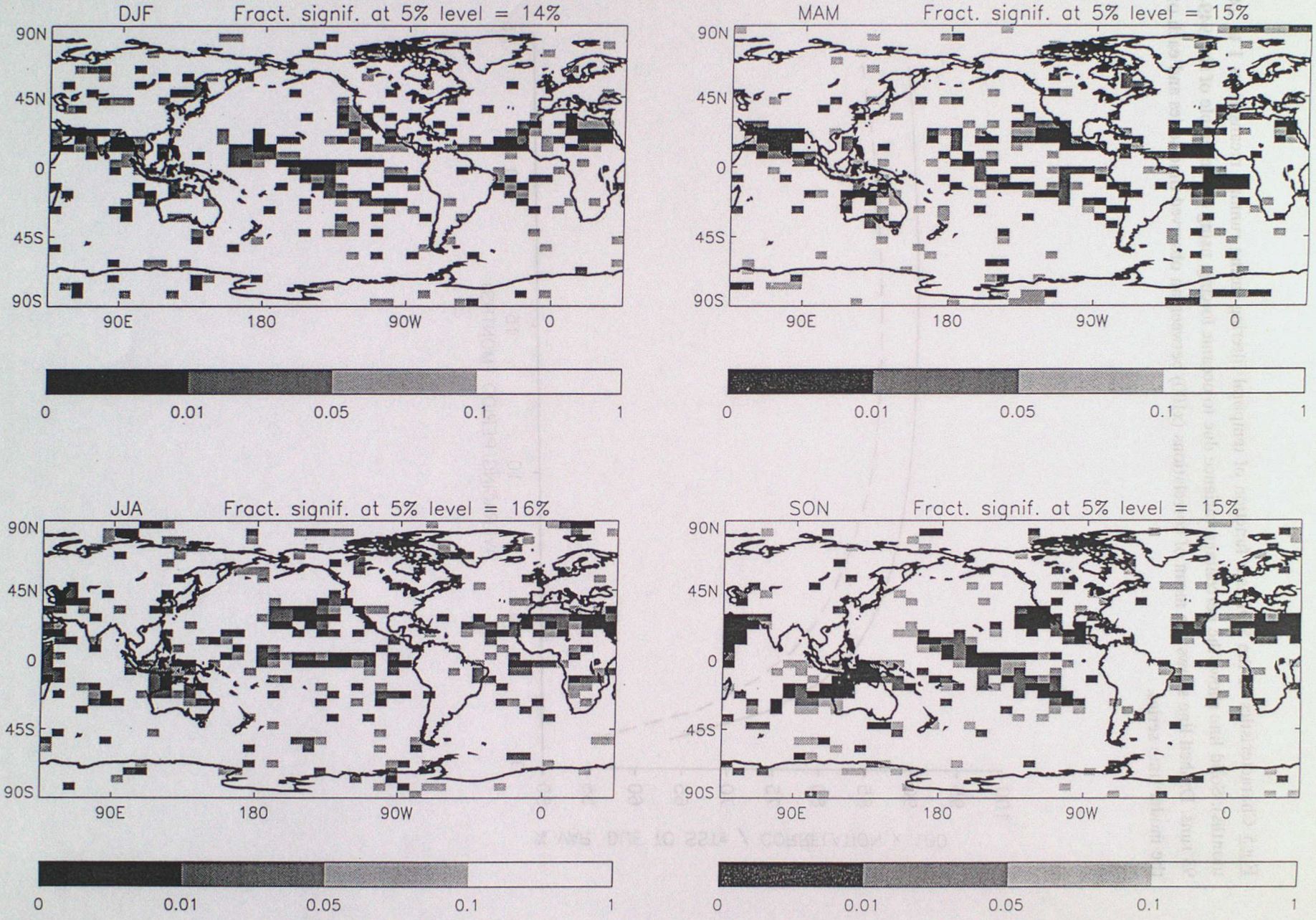

CLIMATE RESEARCH TECHNICAL NOTES

CRTN 1	Oct 1990	Estimates of the sensitivity of climate to vegetation changes using the Penman-Monteith equation. P R Rowntree
CRTN 2	Oct 1990	An ocean general circulation model of the Indian Ocean for hindcasting studies. D J Carrington
CRTN 3	Oct 1990	Simulation of the tropical diurnal cycle in a climate model. D P Rowell
CRTN 4	Oct 1990	Low frequency variability of the oceans. C K Folland, A Colman, D E Parker and A Bevan
CRTN 5	Dec 1990	A comparison of 11-level General Circulation Model Simulations with observations in the East Sahel. K Maskell
CRTN 6	Dec 1990	Climate Change Prediction. J F B Mitchell and Qing-cun Zeng
CRTN 7	Jan 1991	Deforestation of Amazonia - modelling the effects of albedo change. M F Mylne and P R Rowntree
CRTN 8	Jan 1991	The role of observations in climate prediction and research. D J Carson
CRTN 9	Mar 1991	The greenhouse effect and its likely consequences for climate change. D J Carson
CRTN 10	Apr 1991	Use of wind stresses from operational N.W.P. models to force an O.G.C.M. of the Indian Ocean. D J Carrington
CRTN 11	Jun 1991	A new daily Central England Temperature series, 1772-1991. D E Parker, T P Legg and C K Folland
CRTN 12	Jul 1991	Causes and predictability of Sahel rainfall variability. D P Rowell, C K Folland, K Maskell, J A Owen, M N Ward

CLIMATE RESEARCH TECHNICAL NOTES

CRTN 13 Jul 1991 Modelling changes in climate due to enhanced CO2, the role of atmospheric dynamics, cloud and moisture.
C A Senior, J F B Mitchell, H Le Treut and Z-X Li

CRTN 14 Sep 1991 Sea temperature bucket models used to correct historical SST data in the Meteorological Office.
C K Folland

CRTN 15 Aug 1991 Modelling climate change, and some potential effects on agriculture in the U.K.
P R Rowntree, B A Callander and J Cochrane

CRTN 16 Aug 1991 The Boreal Forests and Climate
G Thomas and P R Rowntree

CRTN 17 Aug 1991 Development of a Stratosphere-Troposphere Data Assimilation System.
R Swinbank.

CRTN 18 Sep 1991 A study of asynchronous coupling using a simple climate model.
M K Davey.

CRTN 19 Sep 1991 The Oceanic Carbon Cycle.
N K Taylor

CRTN 20 Nov 1991 Worldwide ocean-atmosphere surface fields in Sahel wet and dry years using provisionally corrected surface wind data.
M N Ward

CRTN 21 Dec 1991 Coupled tropical ocean global atmosphere models at the UKMO.
M K Davey, C Gordon, S Ineson and S Lawrence

CRTN 22 Dec 1991 Empirical parameterisation of tropical ocean-atmosphere coupling.
M Allen, M K Davey, D L T Anderson and P D Killworth

CRTN 23 Feb 1992 The temporal evolution of Equatorial Currents in the Indian Ocean
D L T Anderson, D J Carrington, R A Corry and C Gordon

CRTN 24 Feb 1992 Stratospheric analyses provided by the U.K. Meteorological Office
M J Bailey, A O'Neill and V D Pope

CLIMATE RESEARCH TECHNICAL NOTES

CRTN 25	Feb 1992	Modelling interannual variability in the Indian Ocean using momentum fluxes from the UKMO and ECMWF operational weather analyses. D L T Anderson and D J Carrington
CRTN 26	Mar 1992	A GCM simulation of the impact of Amazonian deforestation on climate using an improved canopy representation J Lean and P R Rowntree
CRTN 27	Mar 1992	The parameterization of rainfall interception in GCMs A J Dolman and D Gregory
CRTN 28	Jun 1992	Development of worldwide marine data eigenvectors since 1985 A W Colman
CRTN 29	Jun 1992	A tropical ocean model with reduced physics M K Davey
CRTN 30	Jun 1992	International Temperature Workshop, Boulder, Colorado, USA, 16 January 1992 Edited by D E Parker
CRTN 31	Jul 1992	Simulation of clear-sky outgoing longwave radiation over the oceans using operational analyses A Slingo and M J Webb
CRTN 32	Sep 1992	A prediction of the transient response of climate J M Murphy
CRTN 33	Nov 1992	LEPS scores for assessing climate model simulations and long-range forecasts. C K Folland
CRTN 34	Jan 1993	Stratospheric Data Assimilation System Guide Editer: R Swinbank
CRTN 35	Mar 1993	A Stratosphere-Troposphere Data Assimilation System R Swinbank and A O'Neill
CRTN 36	Mar 1993	Validation of hydrological schemes for climate models against catchment data. P R Rowntree and J Lean

CLIMATE RESEARCH TECHNICAL NOTES

CRTN 37	Apr 1993	Modelling of palaeoclimates: Examples from the recent past J F B Mitchell
CRTN 38	May 1993	A simulation of seasonality in ENSO forecast skill M K Davey, D L T Anderson and S Lawrence
CRTN 39	Jul 1993	ENSO Prediction experiments using a simple ocean-atmosphere model D-H Wu, D L T Anderson and M K Davey
CRTN 40	Sep 1993	Diagnosis of dynamic sea-surface and sea-level changes from the Cox ocean model J M Gregory
CRTN 41	Sep 1993	Seasonal variations of the clear-sky greenhouse effect: the role of changes in atmospheric temperatures and humidities M J Webb, A Slingo and G L Stephens
CRTN 42	Nov 1993	Sea-level changes under increasing atmospheric CO_2 in a transient coupled ocean-atmosphere GCM experiment. J M Gregory
CRTN 43	Dec 1993	Global and regional patterns of climate change: recent predictions for the Arctic P R Rowntree
CRTN 44	Feb 1994	The effect of changing horizontal diffusion in the atmospheric version of the unified climate model C D Hall and R A Stratton
CRTN 45	Mar 1994	Simulation of El-Niño/Southern Oscillation like variability in a global AOGCM and its response to CO_2 increase. S F B Tett
CRTN 46	Apr 1994	Global data required for monitoring climate change. D E Parker and C K Folland
CRTN 47	May 1994	Seasonal uptake of anthropogenic CO_2 in an ocean general circulation model. N K Taylor

CLIMATE RESEARCH TECHNICAL NOTES

CRTN 48	Jun 1994	A tropic-wide oscillation of boreal summer rainfall and patterns of sea-surface temperature. M N Ward, K Maskell, C K Folland, D P Rowell and R Washington
CRTN 49	Jun 1994	Simulation of the tropical Pacific using a simplified ocean model M A Balmaseda, D L T Anderson and M K Davey
CRTN 50	Sep 1994	Simulation of global mean temperature using a box-diffusion climate model P R Rowntree
CRTN 51	Sep 1994	Seasonal dependence of ENSO prediction skill M A Balmaseda, M K Davey and D L T Anderson
CRTN 52	Nov 1994	Simulation of the Indian Monsoon and Tropical Intraseasonal Variability by a General Circulation Model P M Inness and D Gregory
CRTN 53	Mar 1995	A comparison of modelled surface fluxes with climatological estimates. C Gordon and D K Wright
CRTN 54	Mar 1995	The representation of moist convection in atmospheric models. D Gregory
CRTN 55	Mar 1995	A consistent treatment of the evaporation of rain and snow for use in large-scale models D Gregory
CRTN 56	Apr 1995	Workshop on simulations of the Climate of the Twentieth Century using GISST, 28-30 November 1994, Hadley Centre, Bracknell, UK Edited by C K Folland and D P Rowell
CRTN 57	May 1995	Enhanced shortwave cloud radiative forcing due to anthropogenic aerosols. S E Swartz and A Slingo
CRTN 58	May 1995	The simulation of the tropical oceans in models of different horizontal resolution. C Gordon, D K Wright and C M Roberts
CRTN 59	Sep 1995	The water budget of middle latitude continental regions - a modelling and observational study P R Rowntree
CRTN 60	Sep 1995	Intraseasonal variability of the Indian summer monsoon simulated by the Hadley Centre climate model K Ashok, D Gregory and P M Inness

CLIMATE RESEARCH TECHNICAL NOTES

CRTN 61	Sep 1995	Climate simulations with the Unified Model: AMIP runs C D Hall, R A Stratton and M L Gallani
CRTN 62	Nov 1995	Validation of surface parameters over the oceans in climate simulations with the unified model. C D Hall
CRTN 63	Dec 1995	The GISST2.2 sea surface temperature and sea-ice climatology D E Parker, M Jackson and E B Horton
CRTN 64	Dec 1995	Parametrization of momentum transport by convection. II: Tests in single column and general circulation models. D Gregory, R Kershaw and P M Inness
CRTN 65	Jan 1996	Understanding the sensitivity of a GCM simulation of Amazonian deforestation to the specification of vegetation and soil characteristics. J Lean and P R Rowntree
CRTN 66	Jan 1996	On the efficient calculation of infra-red fluxes and cooling rates using the two-stream equations. J M Edwards
CRTN 67	Jan 1996	The second Hadley Centre coupled ocean-atmosphere GCM: Model description, spinup and validation. TC Johns,RE Carnell,JF Crossley,JM Gregory, JFB Mitchell,CA Senior,SFB Tett and RA Wood
CRTN 68	Feb 1996	The sensitivity of climate simulations to the specification of mixed phase clouds D Gregory and D Morris
CRTN 69	Apr 1996	Using an ensemble of Multi-Decadal GCM simulations ro assess potential seasonal predictability D P Rowell